POST CRITICAL HEAT FLUX HEAT TRANSFER IN A VERTICAL TUBE INCLUDING SPACER GRID EFFECTS

by

EDWARD M. CLUSS, JR.

S.B., Massachusetts Institute of Technology
(1977)

SUBMITTED IN PARTIAL FULFILLMENT
OF THE REQUIREMENTS FOR THE
DEGREE OF

MASTER OF SCIENCE

at the

MASSACHUSETTS INSTITUTE OF TECHNOLOGY

(June 1978)

Signature of Author . . . . . .
Department of Mechanical Engineering, June 2, 1978

Certified by . . . . . .
Thesis Supervisor

Accepted by . . . . . .
Chairman, Department Committee on Graduate Students

POST CRITICAL HEAT FLUX HEAT TRANSFER IN A VERTICAL TUBE INCLUDING SPACER GRID EFFECTS

by

EDWARD M. CLUSS, JR.

Submitted to the Department of Mechanical Engineering on June 2, 1978 in partial fulfillment of the requirements for the Degree of Master of Science.

ABSTRACT

Theoretical and experimental programs were conducted in order to analyze the supplemental heat transfer, induced by a spacer grid, during an upward post critical heat flux flow in a constant wall temperature pipe. A flooding rate of 1 in/sec, equivalent to 18, 720 lbm/hr-ft^2, was studied at atmospheric conditions, with hot wall temperatures of 1000°F, 1100°F, 1200°F and 1300°F. Heat flux versus length data was obtained and compared with theoretical predictions. A modified two phase Dittus Boelter correlation was employed to obtain the steady-state heat transfer coefficients. Both entrance and steady-state experimental values correlated well with this model.

Results indicate that an increase in heat transfer does occur at the spacer and is primarily a combination of two mechanisms:

(1) Increased flow velocity (caused by an area reduction at the spacer) which increases vapor convection and droplet heat transfer.
(2) Radiation to liquid deposited on the spacer.

The first contribution can be modeled as a multiplying factor of the steady-state heat transfer level while the latter is a localized effect occurring only at the spacer. The combination of both effects caused a threefold heat transfer increase or greater at the spacer location for the flows studied. Radiation, which is directly related to the hot wall temperature, becomes the major contribution at higher temperatures.

Thesis Supervisor: Peter Griffith
Title: Professor of Mechanical Engineering

ACKNOWLEDGEMENTS

Financial support for this investigation was provided through a research assistantship, funded by the Nuclear Regulatory Commission.

Some portions of the test apparatus were designed and built during earlier heat transfer research by Thomas Smith and Paul Robershotte. The latter also provided numerous suggestions germane to the initial stages of this project.

Joseph "Tiny" Caloggero and Fred Johnson provided technical advice and assisted in the mechanical construction of the experimental apparatus.

Many thanks to Prudence Young, who typed the final and earlier versions of this report, and to Dave Welland for his painstaking proofreading.

Helpful comments and friendship were always abundant from the guys in my office, Mohamed Benchaita, Yin "Clem" Cheung, Joseph Gonzalez-Rivas, and Baldeo Singh. They made the Heat Transfer Lab an interesting place to work.

Professor Griffith, my advisor, provided me with an abundance of guidance and pertinent advice throughout the duration of this project; but more importantly, always retained his optimism, sense of humor, and patience when they were needed the most.

Last but never forgotten; special thanks go to my parents, who have continually given me their love and support for all of my endeavors. To them I dedicate this, my final effort at M.I.T.

To My Mother,

Claire B. Cluss

And My Father,

Edward M. Cluss

TABLE OF CONTENTS

PAGE

LIST OF FIGURES

LIST OF TABLES

NOMENCLATURE

SYMBOL	DEFINITION
A	Area
Cp	Specific Heat
E	Energy
F	Geometric View Factor
G	Mass Flux
H, h	Enthalpy
H_{fg}	Heat of Vapor
K	Thermal Conductivity
$\dot{m}$	Mass Flow Rate
Nu	Nusselt Number
P	Perimeter, Power
Pr	Prandtl Number
q	Heat Transfer
R	Resistance
Re	Reynold's Number
St	Stanton Number
T	Temperature
t	Time
V	Velocity, Voltage
X	Quality

Greek Symbols	DEFINITION
α	Void Fraction
β	Radiating Fraction of Wall
Δt	Time Difference
ε	Effectiveness, Emmisivity
ρ	Density
σ	Stefan-Boltzman Constant
μ	Viscosity

SUBSCRIPTS	DEFINITION
Cu	Copper
d	Droplet
DB	Dittus-Boelter
DS	Droplets at Spacer
eq	Equilibrium
exp	Experimental
f	Liquid
G	Gross
g	Vapor
homo	Homogeneous
in	Inlet
L	Loss
out	Outlet
PRE	Preheater
RS	Radiation at Spacer
s	Spacer, Saturation
sat	Saturation
SS	Stainless Steel
t	Total
v, vap	Vapor
vs	Vapor at Spacer
w	Wall
x	Local, Distance

SUBSCRIPTS	DEFINITION
1	Perpendicular or Deposition
∞	Steady-State

CHAPTER I:

INTRODUCTION

Man's ever increasing demand for energy coupled with dwindling fossil fuel supplies has produced a sharp increase in the cost of conventional power production and has necessitated a switch to alternate but still reliable energy sources. Consequently, following the second World War, the nuclear power industry experienced extensive growth, with the hopes of providing a cheaper and cleaner method of power production. Recently, fears coupling nuclear energy with nuclear weapons and anxiety over a large scale reactor accident have drastically reduced the industry's rate of expansion. It has become increasingly more apparent that the design and construction of only the safest and most reliable reactors will be acceptable to the majority of the population. This concern and controversy has demanded that both commercial reactor producers and the Nuclear Regulatory Commission (responsible for the licensing of nuclear reactors) be extremely cautious and only apply the most conservative reactor design schemes when safety and long term reliability is the question. To insure this reactor dependability, emergency systems are built to handle the most extreme types of accidents. One such hypothetical crisis is the "loss of coolant accident" or LOCA.

1.1 LOSS OF COOLANT ACCIDENT

The hypothetical loss of coolant accident is a problem highly unlikely to occur but is of great interest as a limiting design case. During this accident, a double guillotine break occurs in the main pipes

of the primary loop causing a rapid depletion of the reactor coolant and extreme depressurization of the reactor core. Figure 1, obtained from Hsu (1), shows that in approximately 30 seconds the pressure can drop from 2300 psig to nearly 50 psig. This subcooled depressurization period is known as the Blowdown stage and has been modeled extensively by Bjørnard (2).

As the rate of pressure drop decreases, the remaining flow may experience several flow reversals, and flashing of liquid into vapor occurs. Due to the high void and low coolant flowrate, dryout occurs on the fuel rod surfaces and the critical heat flux condition is reached. Figure 1 also shows that at approximately 10 seconds after the main pipe's rupture, the emergency cooling system (ECCS) is initiated and water is pumped into the reactor core. When the rising pool of water (traveling typically at 1 in/sec) in the lower plenum reaches the dried out fuel rods, water is boiled and this resulting two phase flow aids in slowly cooling the upper portions of the rods and their structural supports. Eventually the rising pool of water quenches the fuel rods and a quench front propogates upward.

1.2 SPACER GRID EFFECTS

An observation made by Bjørnard (2) and other investigators is that there are discrete locations ahead of the quench front where a limited amount of rewetting has already occurred. These positions correspond to the orientation of fuel rod structural supports, known as spacer grids. Apparently, due to mechanical constrictions and distur-

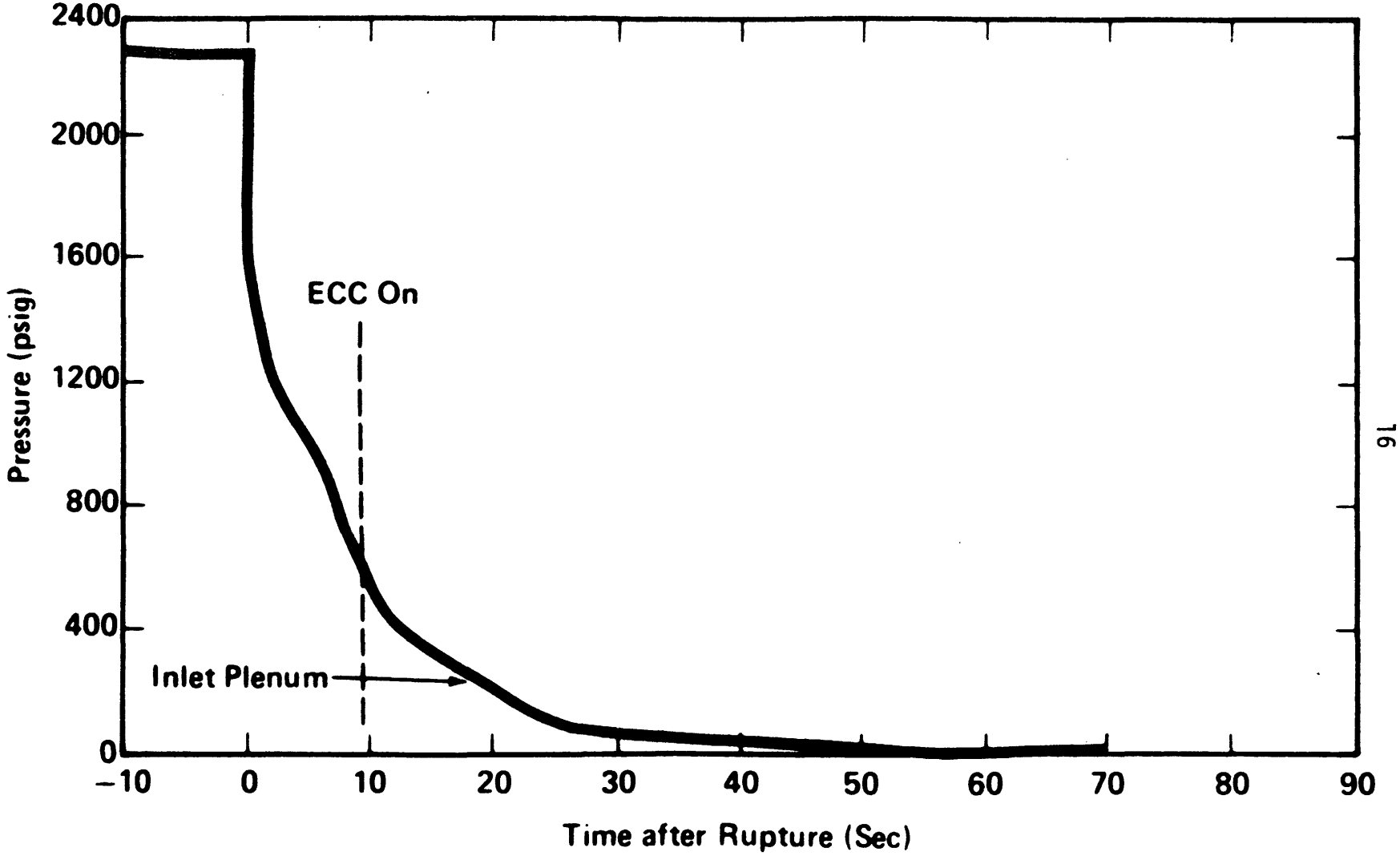

FIGURE 1: PRESSURE HISTORY DURING BLOWDOWN

bances, a beneficial effect which aids in the cooling process has been encountered. Two results, therefore, seem likely. Spacer grids may cause local fuel rod rewetting shortly before the neighboring region quenches, and secondly, the heat transfer may be enhanced at these discrete locations both before and after quenching occurs.

1.3 PREVIOUS EXPERIMENTATION

A great deal of effort and money has been expended to obtain a better understanding of the flow regimes encountered during a LOCA and their corresponding modes of heat transfer. When dryout occurs on the surface of the fuel rods, there is a departure from nucleate boiling. This regime, known as post critical heat flux (or post CHF), is characterized by a violent increase in wall temperature and rapid decrease in the associated heat transfer coefficient. Possible flow regimes that are experienced include inverted annular flow film boiling and dispersed flow film boiling. The latter occurs at higher void fractions. These flow regimes are shown in Figure 2 along with the flow situations encountered prior to CHF.

Experimental and theoretical research has been carried on at MIT for several years. Smith (3) studied heat transfer and void fraction during upflow while Robershotte (4) performed similar heat transfer experimentation and some associated modeling for the downflow situation. An analytical program was developed by Kaufmann (5) to model heat transfer in inverted annular and dispersed flow film boiling during upflow. Bjørnard (2) developed a computer program package which models the entire

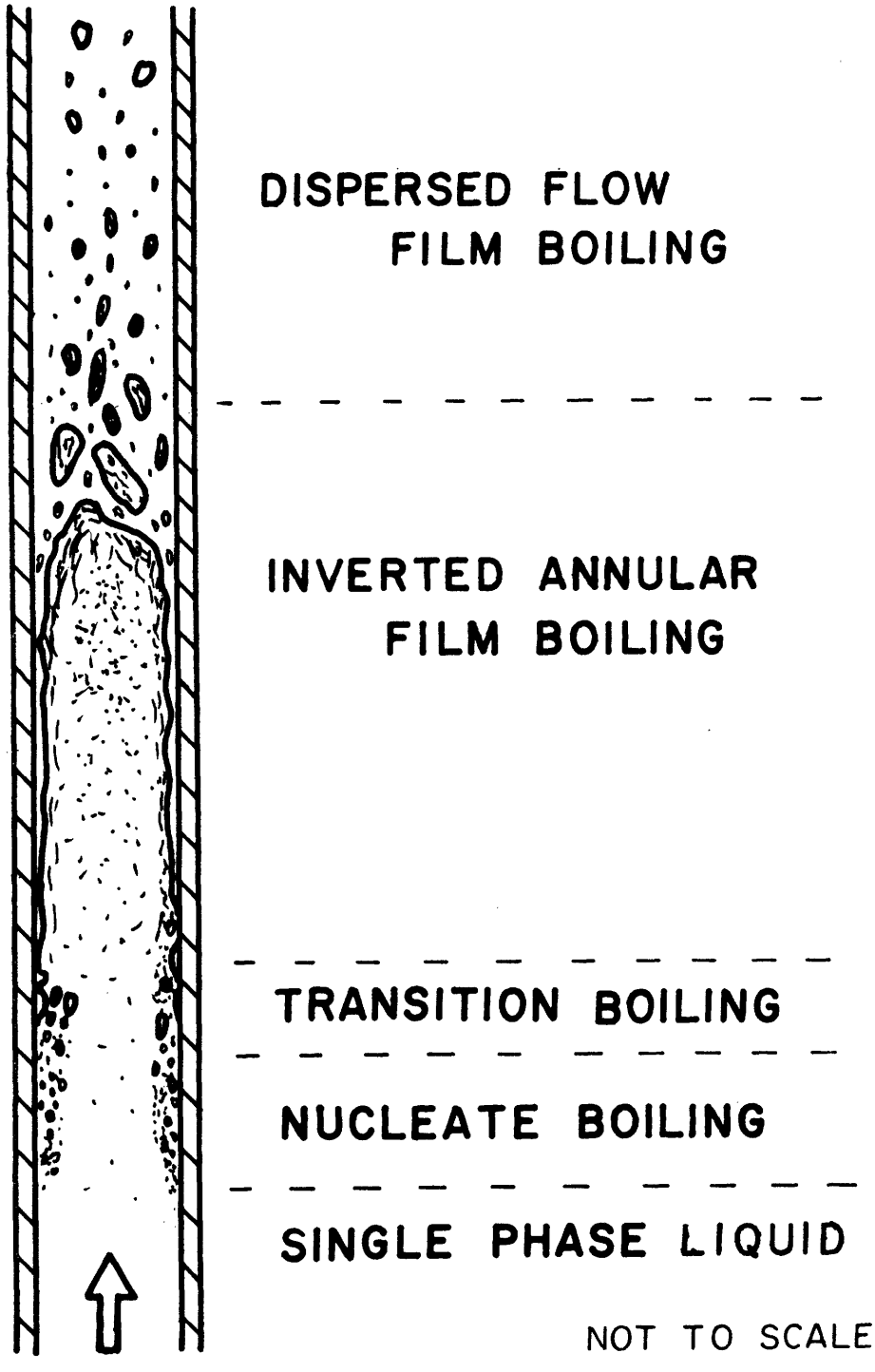

FIGURE 2: TWO PHASE FLOW REGIMES

blowdown stage. Currently, Singh (6) is studying the flow reversal phenomenon, characteristic of the saturated depressurization period following blowdown, and the thermal hydraulics of gravity - feed reflood is being investigated by Cheung (7). Gonzalez-Rivas (8) recently concluded a void fraction and carryover transient analysis.

1.4 OBJECTIVE OF THIS WORK

Virtually no prior experimentation and only minor modeling efforts have been conducted that are directly related to spacer grid effects encountered during the reflood period. As a result, both an experimental and analytical program were developed to investigate this problem. Specifically, upflow will be considered with flow parameters typical of those occurring during reflood. The models employed allow one to make reasonable estimations of the added heat transfer effect of spacer grids during a steady-state, upflow, post critical heat flux situation.

CHAPTER II:

EXPERIMENTAL PROGRAM

2.1 APPARATUS

Equipment employed during this investigation was a combination of that used by Smith (3), Robershotte (4), and additions or alterations performed by the current experimenter. Elaborate efforts were made to insure that the apparatus accurately represents the actual physical situation experienced in a reactor core during a LOCA.

2.1.1 Reactor Model

The reactor core consists of a bundle of fuel rods and control rods in a spacer grid assemblage which provides structural support. When boiling occurs low in the bundle during reflood the resulting two phase flow moves vertically past the rod bundle. This flow, external to the rods was experimentally modeled as a two phase internal flow in a tube by matching the external flow's hydraulic diameter, mass flux and Reynolds number.

At the discrete spacer grid locations, a flow constriction is incurred and droplet interference is encountered. This external flow behavior was also transformed to a corresponding internal model which accounted for the flow area reduction.

The entire experimental system was responsible for providing the correct inlet flow conditions to a constant wall temperature section, which included the spacer model.

2.1.2 Test Loop Description

A schematic of the entire experimental apparatus is shown in Figure 3 and photographs are presented in Figures 4 and 5. At the start of a cycle, water left a reservoir tank and proceeded, via copper tubing, to a 10 gallon per minute capacity centrifugal pump. Due to the pump's over production, most of the liquid was immediately recycled around it through a bypass valve. The water continuing forward passed through a Fulflo SSHP-2416 filter and was then monitored with a float type flowmeter (Tube #FP-1/2-27-6-10/55, Float #GUSVT-40T60). Fine adjustments of the flow rate were made by valves located at either end of the flowmeter.

Water next entered a shell and tube 40 psi steam preheater in order that the liquid subcooling be reduced. A recirculating valve was employed during start up operations in order that thermal time constants be reduced in the main test section. During steady state operation, however, all of the liquid traveled past the recirculating valve and through the four-way valve, advancing towards the electric preheater. The electric preheater, a 3/8 inch 304 stainless steel pipe (.675 inch O.D., .493 inch I.D.) was heated with a direct current generator capable of producing 45 KW of power. Although a fraction of this power output was required, the cables connecting the preheater and generator were water cooled. A photograph of the electric preheater appears in Figure 6. Voltage was measured directly across the electric preheater; whereas current measurements were obtained from the voltage drop across a cali-

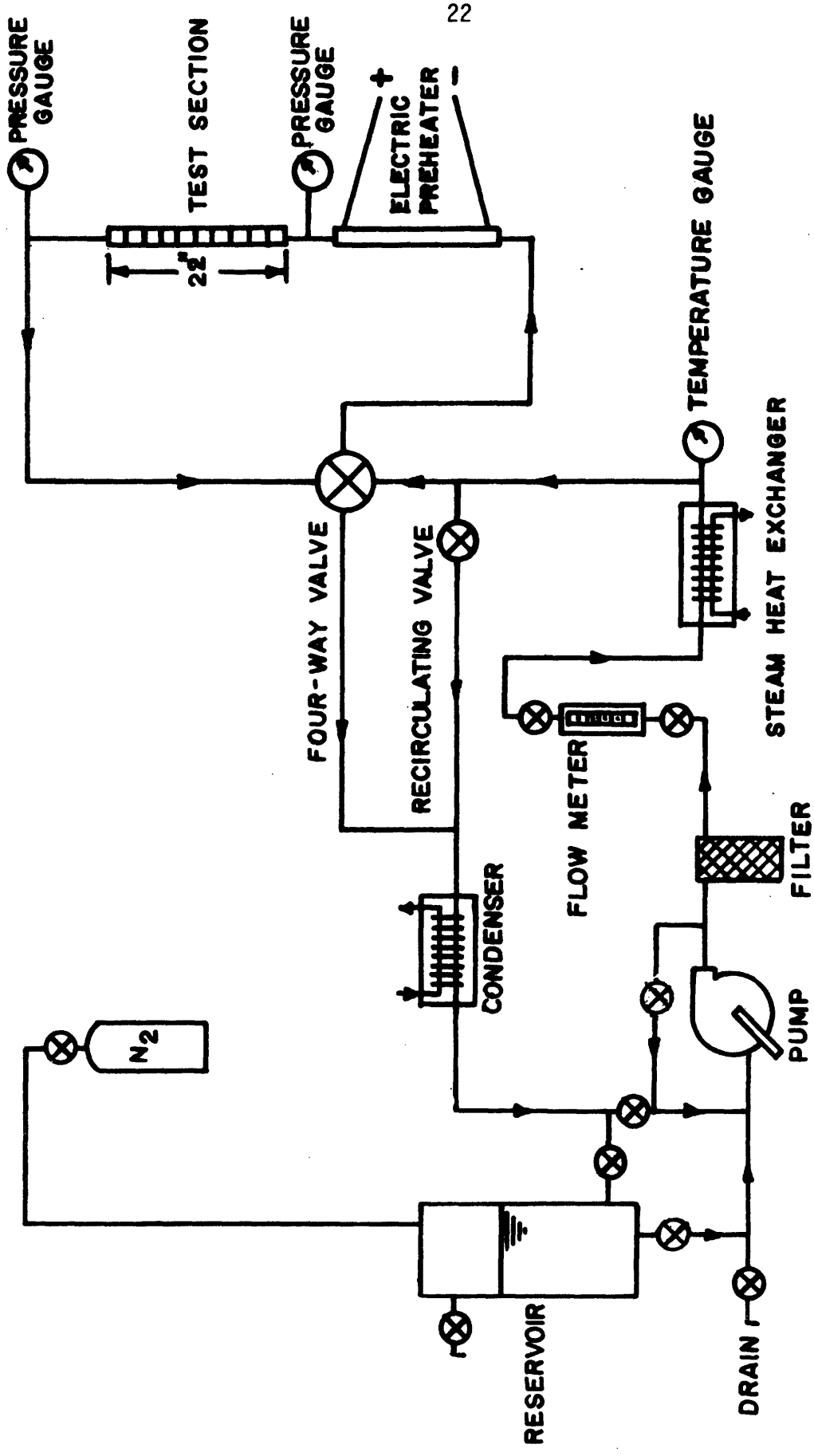

FIGURE 3: SCHEMATIC OF EXPERIMENTAL APPARATUS

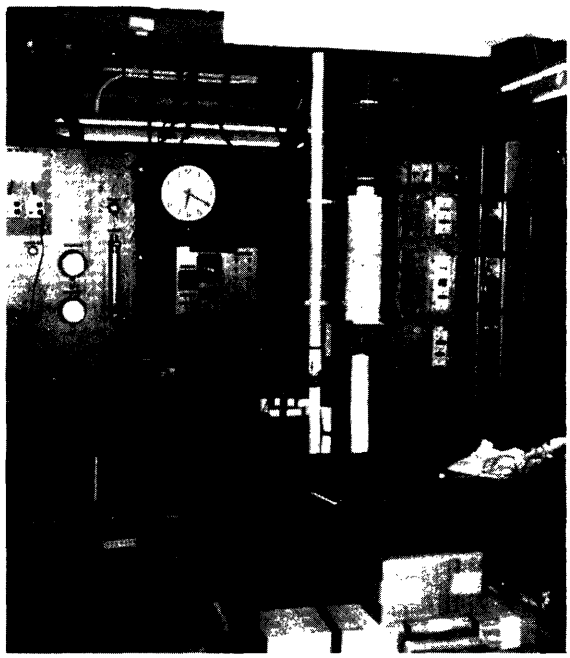

Figure 4. Entire Apparatus

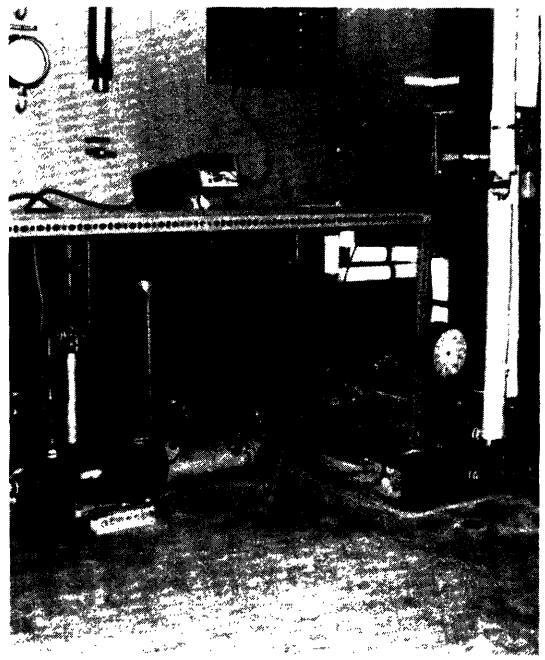

Figure 5. Lower Portion of Apparatus

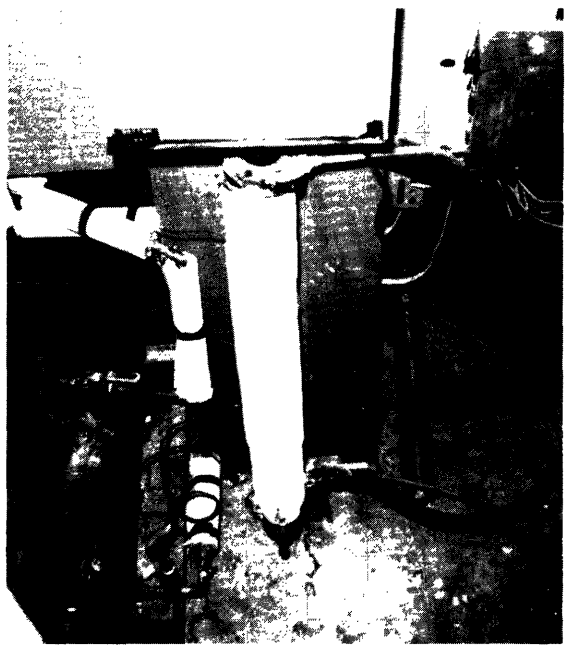

Figure 6. Electric Preheater

Figure 7. Pipe Connector

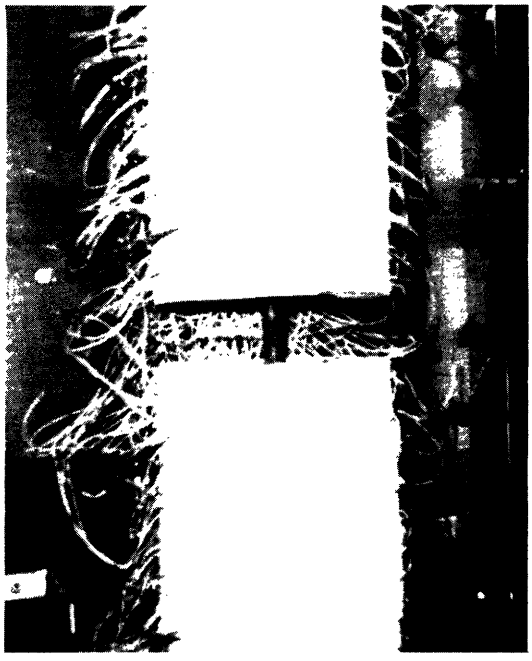

Figure 8. Pipe Without Copper Block

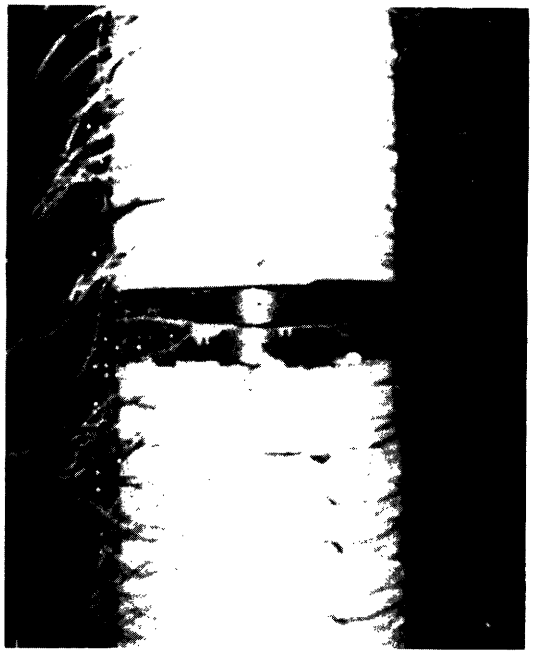

Figure 9. Pipe with Copper Block

Figure 10. Test Section Wiring

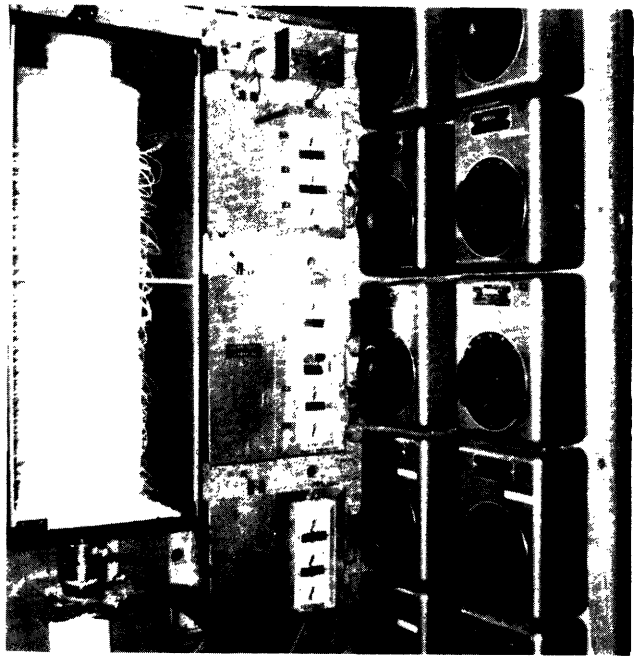

Figure 11. Environment Chamber, Controller Clocks, and Variacs

brated NBS shunt resistor located on the generator console. Teflon disks (1/16 inch thick) inserted in a specially produced pipe connector shown in Figure 7, electrically insulated the preheater from the neighboring test loop elements. Constant monitoring of the preheater's power level and temperature were required to guard against pipe burnout and rupturing since this was a constant heat flux mode of heat transfer.

The low quality steam produced in the electric preheater then entered the main test section, wall temperature of which was controlled and set at a constant temperature. Heat, added to maintain the fixed wall temperature, was measured and recorded in order that heat flux versus length data could be obtained. A more complete explanation of the components involved in this process will be presented in the next two sections. Steam, exiting from the main test section, re-entered the copper tubing network and was desuperheated and subcooled in a condenser. Liquid produced in the condenser, returned to the system reservoir and awaited further recycling.

2.1.3 Test Section Components

The test section consisted of a 304 stainless steel pipe with a "spacer" internally welded to it. All instrumentation and related components were located along a 22 inch stretch of the pipe; however, a short entrance length and longer exiting one increased the pipe's overall length to 34 inches. The spacer, shown in Figure 12, was welded at the 11-1/4 inch mark along this 22 inch stretch, in order that a steady-state flow could be established both before the spacer and downstream of it. Figure 17, in Chapter 3, illustrates the spacer with a

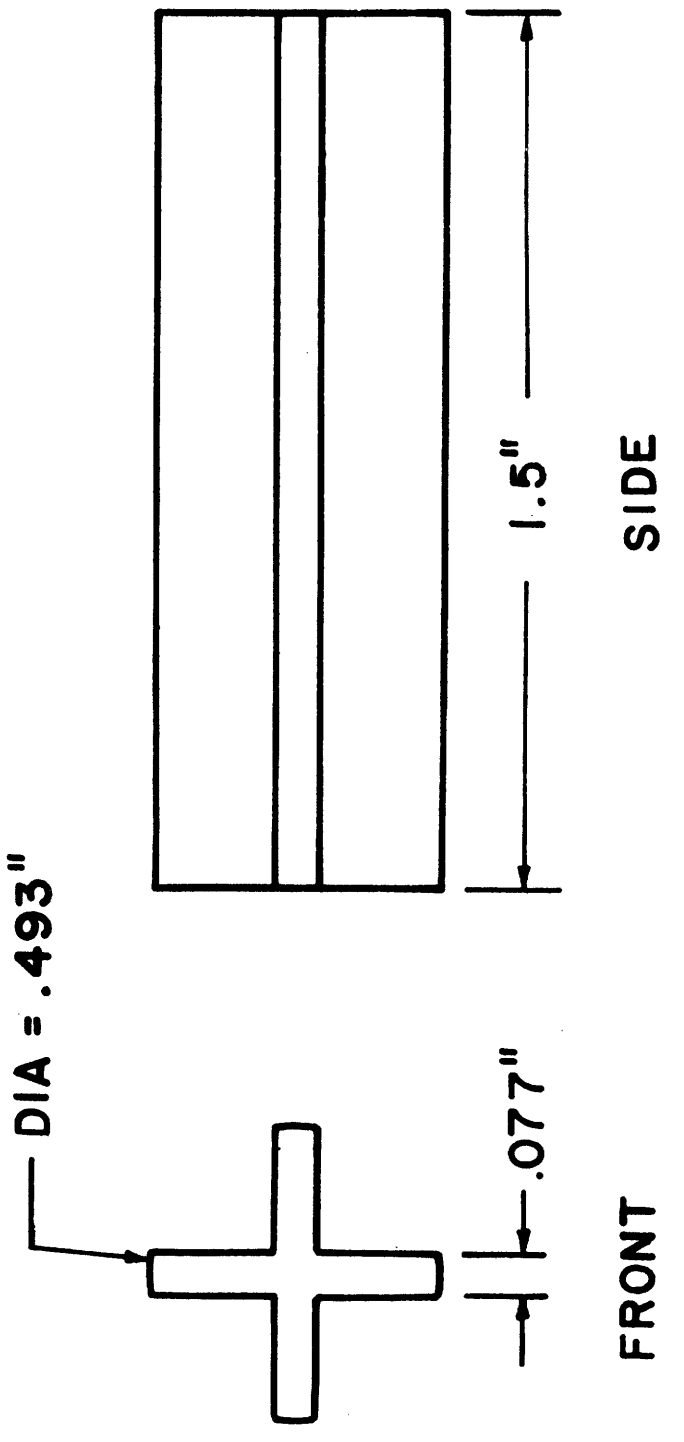

FIGURE 12: EXPERIMENTAL SPACER

portion of the stainless steel pipe wall.

Direct contact conduction heating from hot copper blocks supplied the test section with the required heat flux spikes along its length. The copper blocks were made from 4 inch diameter cylindrical copper, which was cut into 120° sectors and held tightly against the stainless steel pipe with hose clamps. Copper block heights of 7/8 inch, 1-7/8 inch, and 2-7/8 inch were employed with gaps averaging 1/8 inch between neighboring blocks. Holes were drilled and reamed radially into the blocks, 1 inch apart vertically and separated by 40° circumferentially. Figures 8 and 9 show the stainless steel pipe before and after mounting a copper block. Details of a 1-7/8 inch block are illustrated in Figure 13.

Pressed into the radially drilled holes and supplying heat to the copper blocks were 1/4 inch diameter, 1-1/2 inch long, Hotwatt AC resistance cartridge heaters. Each heater was capable of delivering up to 120 watts individually and 198 heaters were uniformly distributed over the 22 inch length. Voltage supplied to the cartridge heaters originated from 10 variable transformers (Variacs), each with a 140 volt/10 amp power potential. A total of 10 copper blocks (30 sections) were used such that there was a one to one correspondence between blocks and variacs. This enabled the power delivered to each block to be independently determined and ten individual heat flux spikes established. Since more experimental accuracy is desired at the spacer, shorter copper blocks were located nearby. Hence, there were two 7/8 inch length blocks used by the spacer and four each of the larger two sizes elsewhere.

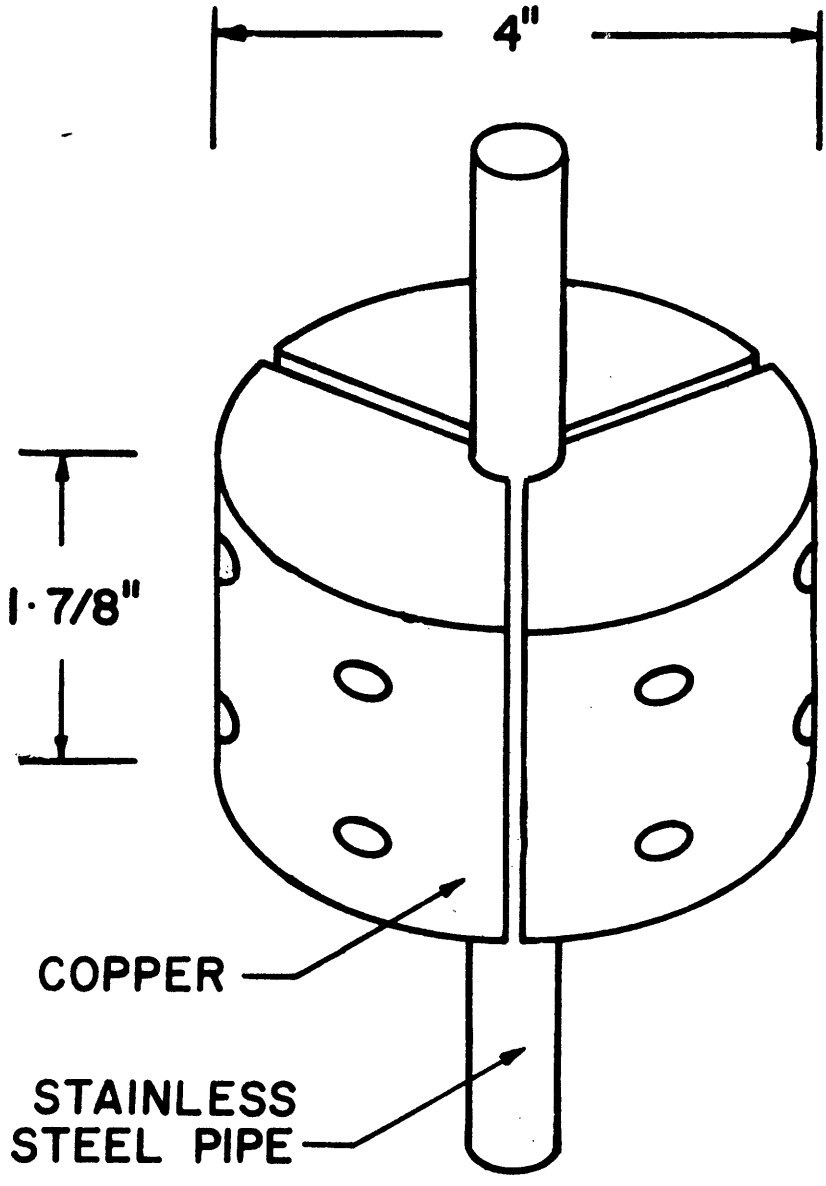

FIGURE 13: DETAILS OF 1-7/8 INCH COPPER BLOCK

This assortment, including gaps, accounted for the 22 inch total length. Surrounding the block assemblage and blanket of asbestos insulation was an aluminum environment chamber with pyrex windows. This box was filled with nitrogen and served to reduce oxidation of the copper blocks.

2.1.4 System Monitoring and Control

Instrumentation was primarily concerned with monitoring and establishing a constant wall temperature in the test section. Temperature readings were obtained using chromel-alumel thermocouples throughout the entire assemblage. At the test section, a total of 30 thermocouples were employed, 3 each at 10 different axial positions. The locations were chosen such that each thermocouple corresponded to one of the 30 copper block pieces. Grooves were cut into the stainless in order to recess the thermocouples inside of the pipe wall, as shown in Figure 14, and insulation was packed on top to insure accurate readings. All 30 thermocouples were monitored and of these, 10 also served as the initial link in the closed loop constant wall temperature controller.

Ten temperature controller circuits (one per block) each compared a different block's thermocouple output to a reference voltage which was set to correspond to the desired wall temperature. A comparator turned a power relay on if the temperature measured was 10°F below the reference point and turned the power relay off if the temperature measured was 10°F above it. The power relay performed two tasks. One, it determined whether current could flow through a Variac and hence if power would be delivered to the block, and two, it turned a sweep hand

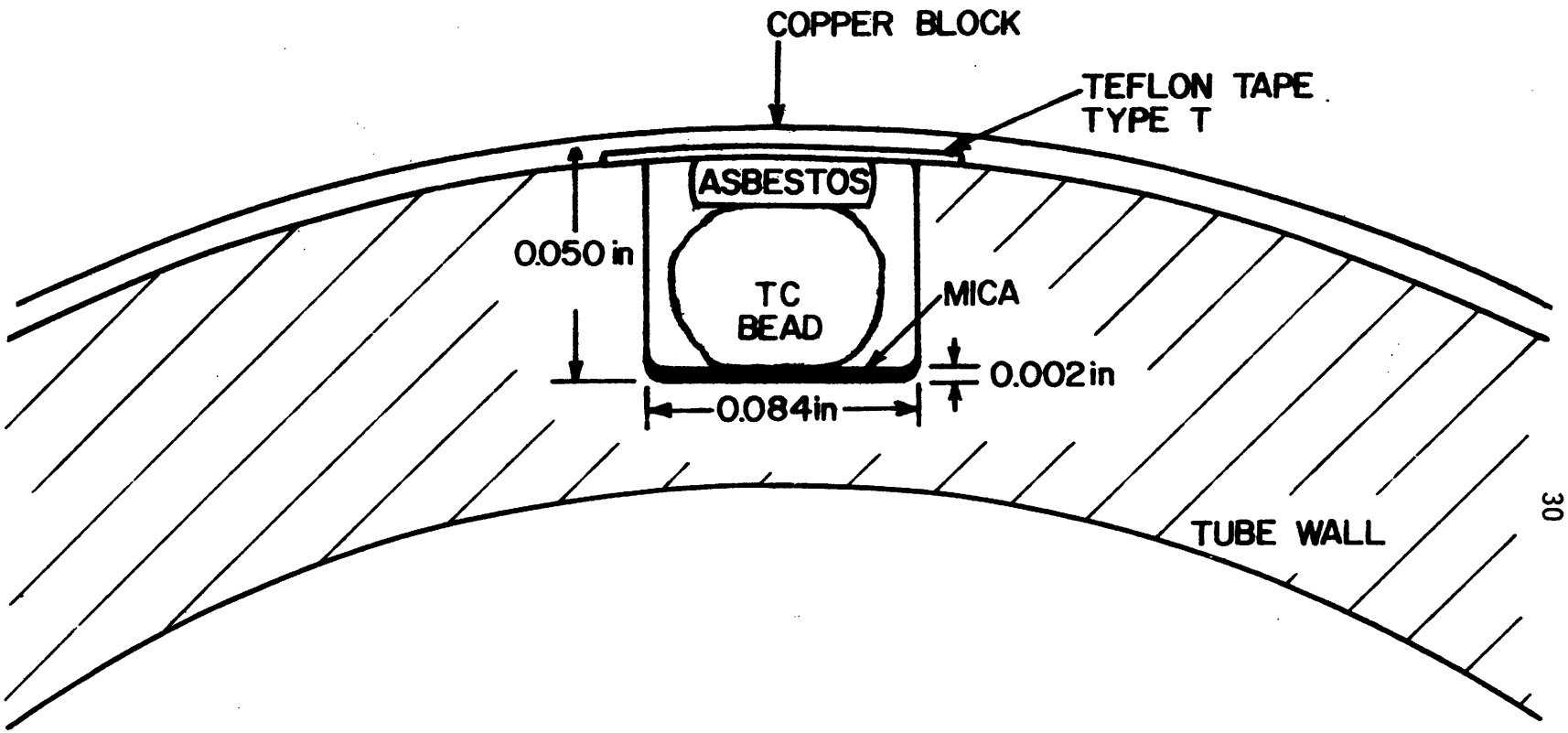

FIGURE 14: MOUNTING OF THERMOCOUPLES

clock on and off which measured the duration of power flow. A circuit diagram of this controller, originally designed by Robershotte (4), is presented in Appendix, A, Figure 26. Photographs of the electrical connections between the test section and terminal blocks; and the environment chamber, controller clocks, and Variacs are shown in Figures 10 and 11. Due to the comparitor's hysterisis and the Variac's voltage setting, a duty cycle resulted which required a 20 minute total run time for proper averaging. Since the voltage level of a Variac was kept constant during any given run, the total energy transferred to a block is simply:

$$E = P\Delta t \tag{2.1}$$

where P is the constant power delivered to the cartridge heaters when the variac is on and Δt is the time recorded on the clock. The gross heat flux then for a 20 minute run is:

$$(q/A)_G = E/A_t(20) \tag{2.2}$$

where A_t is the inside area of the tube.

2.2 EXPERIMENTAL PROCEDURE

A standard procedure was followed for each individual run executed with the apparatus. A cursory description of the steps involved will be presented here and a tabular form may be consulted in Table 1.

Initially, a desired wall temperature was chosen and the corresponding controller reference voltage set. Estimates of the test section

TABLE 1

EXPERIMENTAL PROCEDURE

I. Initial Preparation

1) Choose desired wall temperature and set corresponding controller reference voltage

2) Estimate test section power requirements and set Variac voltage level

3) Calculate required amount of preheating

4) Reset clocks

II. Start Up Operations

1) Open condenser and cooler water valves

2) Bleed nitrogen into environment chamber

3) Open recirculation and steam valves

4) Turn pump and test section power on

5) Check thermocouples and flowrate

6) When test section obtains desired temperature, close recirculating valve and turn electric preheater on.

III. Steady-State and Shutdown Procedure

1) Turn clocks on

2) Monitor and record flow rate, preheater power level, and temperatures

3) Shut down system and turn off clocks after 20 minutes

4) Record elapsed time on clocks, Variac voltages, cartridge resistances, etc.

power requirements were made and Variacs turned to the proper voltage levels. Also calculations pertinent to the flow's quality (and hence Reynolds Number) were made in order to determine the required amount of preheating.

During start up operations, the generator cable coolant and condenser water were allowed to flow and nitrogen was bled into the environment chamber. Next the recirculation valve and steam valve were opened; and the pump and test section power turned on. The flow rate was established while the thermocouples were being monitored. Once the test section obtained its desired temperature, the recirculating valve was closed and the electric preheater turned on.

After the entire system reached steady-state, the clocks were turned on the the run was begun. During the following 20 minutes, the flowrate, preheater power level, and temperatures were monitored and adjusted accordingly. When the run was completed, the time elapsed on each clock was recorded; and resistance measurements of the cartridge heaters conducted, testing for burnouts. Also the flowrate, wall temperature, variac settings, preheater power level and observations were noted for data reduction and further analysis.

2.3 DATA REDUCTION

The total average power to each block is equal to the rate of energy dissipation in the cartridge heaters. The total resistance of n parallel heaters in a given block is R_t, where:

$$\frac{1}{R_t} = \sum_{i=1}^{n} \frac{1}{R_i} \tag{2.3}$$

The gross heat transfer rate, then, is dependent on this resistance, a Variac's voltage setting, and the ratio of time on to the total run time.

$$q_G = \left(\frac{V^2}{R_T}\right) \left(\frac{t_{on}}{t_{run}}\right) (3.412) \qquad (2.4)$$

where 3.412 is a conversion factor from Watts to Btu/hr.

Not all of this gross energy transfer directly heats the test section. Some energy is lost to the environment and thermal capacitance effects may occur in the stainless steel pipe or copper blocks.

$$q_G = q_{net} + q_L + \left[(\dot{m}Cp)_{SS} + (\dot{m}Cp)_{Cu}\right] \frac{dT}{dt} \qquad (2.5)$$

Due to the cyclis nature of the heating process and steady state conditions; however,

$$\int_o^t \frac{dT}{dt} = o \qquad (2.6)$$

This reduces Equation 2.5 to:

$$q_{net} = q_G - q_L \qquad (2.7)$$

Heat losses to the environment were measured before each run and deducted from the calculated gross heat transfer, yielding the net heat transferred to the test section. Knowing q_{net}, an experimental heat transfer coefficient could be obtained with $A = A_t$.

$$h_{exp} = \frac{(q/A)_{net}}{(T_{wall} - T_{sat})} \tag{2.8}$$

It is also necessary to know the entering equilibrium quality and hence, also the entering enthalpy to the test section. Since the fluid temperature entering the preheater, T_{ent}, was known, the amount of superheat enthalpy was calculated from an energy balance at the electric preheater

$$H_{in} = (T_{in} - T_{sat}) + \frac{q_{PRE}}{\dot{m}} \tag{2.9}$$

The difference in temperature between T_{in} and T_{sat} in Equation 2.9 represents the amount of enthalpy required to eliminate the subcooled liquid. The equilibrium quality entering the test section is then,

$$(X_{eq})_{in} = \frac{H_{in}}{H_{fg}} \tag{2.10}$$

The inlet equilibrium quality can not be calculated for subsequent blocks using

$$X_{eq}^{(i+1)} = \frac{q_{net}^{(i+1)}}{(\dot{m})(H_{fg})} + X_{eq}^{(i)} \tag{2.11}$$

which is an energy balance performed on each test section increment.

CHAPTER III:

THEORETICAL ANALYSIS

3.1 POST CHF HEAT TRANSFER

During an analysis dealing with a two phase flow, proper identification must be made of the equivalent single phase properties. In this investigation, an effective equilibrium vapor Reynolds Number is applied which incorporates the mass flux, quality, and void fraction:

$$Re_v = \frac{GD\ X_{eq}}{\alpha\ \mu_v} \tag{3.1}$$

The vapor flow is considered turbulent when $Re_v > 3000$. In the dispersed flow region, α is approximately equal to 1.0, indicating that the void fraction may be neglected when testing for turbulence. Thus, turbulent flow occurs when

$$\frac{GD\ X_{eq}}{\mu_v} > 3000 \tag{3.2}$$

The total heat flux in this situation is the result of two contributions.

$$(q/A) = (q/A)_v + (q/A)_d \tag{3.3}$$

The first term, $(q/A)_v$, represents wall to vapor forced convection heat transfer; while $(q/A)_d$ is the wall to droplet mode of heat transfer.

3.1.1 Forced Convection Heat Transfer to Vapor

Dittus-Boelter (9) correlated data for a forced convection single phase flow in a pipe and established an empirical equation for a heat transfer coefficient. In this two phase study, the single phase Reynolds Number used by Dittus-Boelter is replaced by the effective Reynolds Number in Equation 3.1 yielding:

$$h_{DB} = (.023) \frac{K_v}{D} (Re)_v^{.8} (Pr)_v^{.4} \qquad (3.4)$$

Since thermal equilibrium is not insured, this heat addition can either increase the quality or superheat the existing vapor. If no superheating occurs (typical of higher mass velocities), and equilibrium model may be employed.

$$(q/A)_v = h_{DB} (T_{wall} - T_{sat}) \qquad (3.5)$$

Vapor properties are evaluated at the saturation temperature. During lower mass velocities, however, a model which assumes only superheating is more accurate. In this case, vapor properties are calculated at the actual vapor temperature.

$$(q/A)_v = h_{DB} (T_{wall} - T_{vap}) \qquad (3.6)$$

Equation 3.5 is known as the "Equilibrium Model" or "Dougall-Rohsenow Limit", while Equation 3.6 is called the "Fixed Vapor Fraction Model" or

"Fixed Gx Model". The present investigation utilizes the latter model, since flows with mass velocities typically encountered during reflood in a reactor have been modeled more successfully with this formulation (4). This decision, however, is not of great consequence, since use of the equilibrium model would only slightly alter the primary results being sought.

The vapor temperature is found by performing a control volume heat balance on a test section increment. Heat entering the vapor is simply,

$$q_v = (x\,\dot{m})\, C_p\, (T_{out} - T_{in}) \tag{3.7}$$

The mean value of the inlet and outlet temperatures is the vapor temperature;

$$T_{vap} = (\tfrac{1}{2})\, (T_{in} + T_{out}) \tag{3.8}$$

This scheme, which calculates T_{vap}, is an iterative one, since the vapor properties used to evaluate Equation 3.4 for the heat transfer coefficient are dependent on this temperature. It is necessary to first estimate the vapor temperature, then evaluate the vapor properties, calculate the heat transfer coefficient, and apply Equation 3.6. Next, an energy balance is conducted with Equations 3.7 and 3.8 yielding an updated approximation for the actual vapor temperature. Only a few iterations are required with this method and convergence is quickly obtained.

The method of evaluating the wall to vapor heat transfer assumes a fully-developed flow. Since a development length will be experienced, entrance effects must be accounted for. Figure 15, reproduced from ESDU (1968) (10), gives plots of three entrance effects based on different entrance configurations. This figure shows the ratio of the local Stanton Number to the fully developed value, where

$$St_x = \frac{Nu_x}{RePr} = \frac{h_x D}{k\,RePr} \tag{3.9}$$

The actual heat transfer coefficient compared to its fully-developed value is proportional to the corresponding Nusselt numbers, and hence, also to the Stanton quantities.

$$\frac{h_x}{h_\infty} = \frac{Nu_x}{Nu_\infty} = \frac{St_x}{St_\infty} \tag{3.10}$$

Apparatus utilized in this research (see Chapter II) used an electrically insulating pipe coupler, which behaves like an orifice to the flow. A short calming distance of four inches is then encountered followed by a jump in temperature at the heated section, as illustrated in Figure 16. Although none of the entrance configurations exactly match this situation, cases 2 and 3 provide a range in which the anticipated entrance effects should lie.

3.1.2 Wall to Droplet Heat Transfer

The second and less pronounced mode of heat transfer in

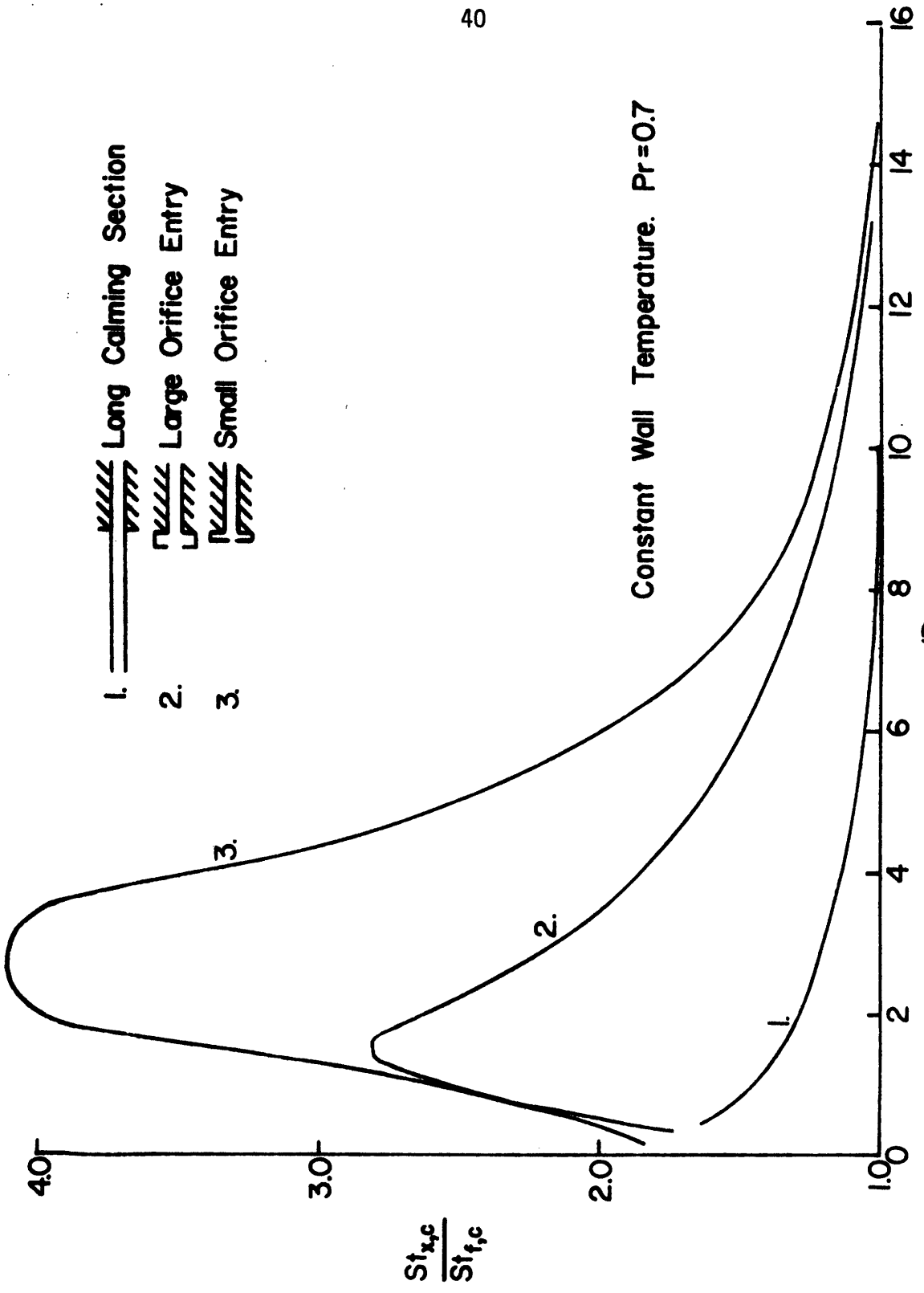

FIGURE 15: EFFECT OF ENTRANCE CONFIGURATION ON LOCAL STANTON NUMBER

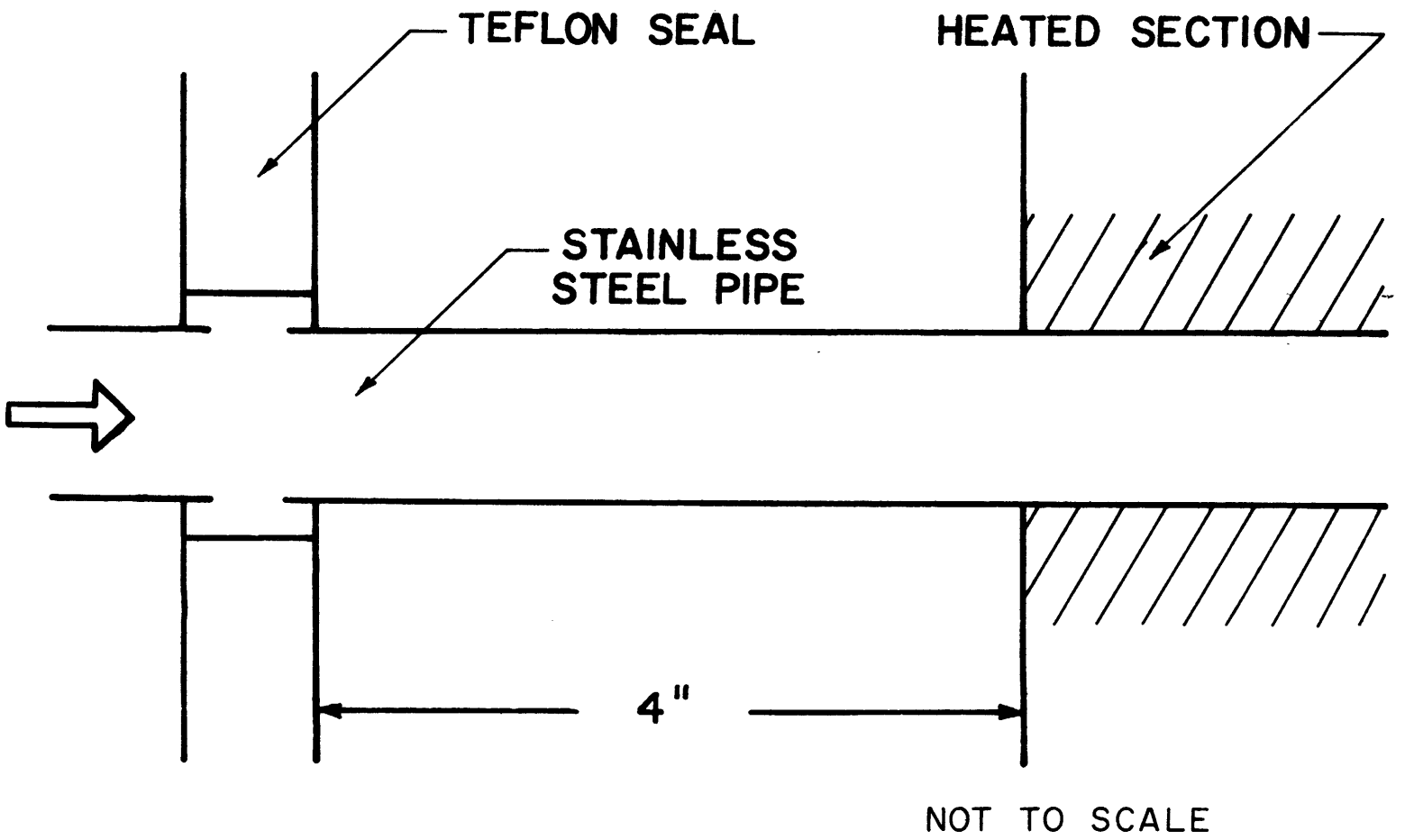

FIGURE 16: TEST SECTION INLET CONFIGURATION

Equation 3.3 is the wall to droplet heat transfer term, $(q/A)_d$. An elusive quantity to obtain despite recently intensified research programs, this contribution is due to droplet evaporization upon entering the vapor boundary layer. A single droplet analysis was performed by Ganic (11), resulting in an expression for the wall to droplet heat flux term;

$$(q/A)_d = (1-\alpha)\ \rho_f\ H_{fg}\ V_1\ \epsilon \qquad (3.11)$$

where α is the void fraction, ρ_f, the liquid density, H_{fg}, the heat of vaporization, V_1, the perpendicular or deposition velocity, and ϵ, the effectiveness or percentage of drop evaporization. Due to the single droplet model, this expression has a high void requirement. If the void were to significantly decrease, droplets colliding with other droplets would begin reducing the actual droplet and wall interaction. Hence, the major restriction placed on Equation 3.11 is that it not be applied when voids are less than 98%. A second limitation is that there be enough vapor to ensure a turbulent dispersed flow.

To fully understand Equation 3.11, each term must be individually defined. The most common definition employed for the void fraction during upflow is the homogeneous model, where the liquid velocity is assumed equal to the vapor velocity due to the interfacial drag force.

$$\alpha_{homo} = \frac{1}{1 + \left(\frac{1-x}{x}\right)\left(\frac{\rho_g}{\rho_f}\right)} \qquad (3.12)$$

Liquid density and heat of vaporization are determined by the system's temperature and pressure. The deposition velocity was determined to be a function of vapor velocity and vapor Reynolds Number by Liu (12).

$$V_1 = (.0289)\, V_v\, (Re)_v^{-.125} \tag{3.13}$$

Effectiveness, ϵ, perhaps the most difficult value to pinpoint, was investigated extensively by Kendall (13). Although lengthy empirical expressions were obtained, a constant value assigned to the effectiveness still seems adequate.

$$\epsilon = .004 \tag{3.14}$$

Considering Equation 3.11 once more, we see that the strongest influence on the wall to droplet heat flux is the void fraction. Hence, within the correlation's limitations, the wall to droplet heat transfer contribution will substantially increase in magnitude, as the liquid fraction rises or the void fraction is lowered.

3.2 SPACER GRID EFFECTS

Numerous causes of increases in total heat transfer at a spacer grid seem likely. Effective area reductions which constrict the flow, increase the flow velocity for a short distance and create an entrance effect at the spacer. This would tend to increase both the wall to vapor convection and wall to droplet conduction. Droplets inpacting the spacer form a saturated liquid boundary layer, which may desuperheat

the vapor, provide some fin cooling, splash drops onto the hot pipe wall downstream, and furnish the hot wall with an available radiation sink. The desuperheating effect is minor since vapor superheating is minimal. Droplet splashing and fin effects cannot be measured and quantified in this investigation but are not considered as major modes of heat transfer. The remaining mechanisms mentioned include increased velocity vapor convection, increased velocity droplet conduction, and wall to spacer radiation.

$$(q/A)_s = (q/A)_{VS} + (q/A)_{DS} + (q/A)_{RS} \tag{3.15}$$

These individual contributions will now be examined in greater detail.

3.2.1 Increased Flow Velocity

Based on mass continuity, the increased mass flux and flow velocity, due to area reduction at the spacer, can be determined:

$$\dot{m} = \dot{m}_s \tag{3.16a}$$

$$GA = G_s A_s \tag{3.16b}$$

$$G_s = G\left(\frac{A}{A_s}\right) \tag{3.16c}$$

The mass flux at the spacer is then related to the upstream and downstream mass flux simply by the area ratio. Also, since the flow density is assumed to remain constant, we have:

$$V_s = V\left(\frac{A}{A_s}\right) \tag{3.17}$$

Due to the increased mass flux, decreased flow area, and also a changed hydraulic diameter, the vapor Reynolds Number must be modified at the spacer location.

$$(Re)_v = \frac{G_s D_s X_{eq}}{\mu_v} \tag{3.18}$$

The hydraulic diameter, D_s, is obtained by considering the actual flow area and the wetted perimeter;

$$D_s = \frac{4A_s}{P} \tag{3.19}$$

These alterations are now substituted into Equations 3.4, 3.6, 3.11 and 3.13, yielding the governing relationships required for determining the vapor convection and droplet conduction heat transfer contributions at a spacer grid.

$$(h_{DB})_s = (.023) \frac{K_v}{D_s} (Re)_s^{.8} (Pr)_v^{.4} \tag{3.20a}$$

$$(q/A)_{vs} = (h_{DB})_s (T_{wall} - T_{vap}) \tag{3.20b}$$

$$(V_l)_s = (.0289) V_s (Re)_s^{-.125} \tag{3.21a}$$

$$(q/A)_{DS} = (1-\alpha) \rho_f H_{fg} (V_l)_s \epsilon \tag{3.21b}$$

3.2.2 Wall to Spacer Radiation

Droplets moving with the vapor flow collide with the spacer grid and become entrained on its surface. Newly formed droplets splash off the rear of the spacer as the liquid boundary layer builds up and periodically erupts. At all times, however, the spacer is wetted by the liquid and remains at the saturation temperature. Due to the large magnitude in temperature difference between the fuel rods and spacer grids during the CHF period and the low flooding rates typically encountered in reflood, a very significant portion of the overall heat transfer experienced at the spacer is expected to be radiation induced.

An important step in quantitatively analyzing the radiation contribution is to properly understand the geometry. Reviewing Figure 8 in Chapter II, the configuration presented is simply a thick cross bounded by a circular wall. Only the pipe wall section not in contact with the spacer, A_w, is able to radiate energy. For this gray body radiation, the governing net heat transfer equation developed by Hottel (14) is,

$$q_{wf} = A_w \mathcal{F}_{wf} \sigma (T_w^4 - T_f^4) \tag{3.22}$$

where the subscripts w and f denote wall and liquid respectively, temperatures are measured in degrees Rankine, $_{wf}$ is the gray body effective view factor, and σ is the Stefan-Boltzman constant,

$$\sigma = \frac{0.1713 \times 10^{-8} \text{ Btu}}{\text{ft}^2 \text{ hr } R^4} \tag{3.23}$$

Assuming nonrefracting surfaces encompassing a nonabsorbing medium,

$$\mathcal{F}_{wf} = \frac{1}{\frac{1}{F_{wf}} + \left(\frac{1}{\varepsilon_w}\right) - 1 + \frac{A_w}{A_f}\left(\frac{1}{\varepsilon_f} - 1\right)} \tag{3.24}$$

Where ε_w is the emissivity of the hot oxidized stainless steel wall, ε_f is the emissivity of the saturated liquid, and F_{wf} is the geometric viewfactor from the radiating wall to the spacer. To obtain F_{wf}, Figure 8 is idealized by straightening the curved surface as illustrated in Figure 17. Due to symmetry, only one quarter of this configuration need be considered in order to evaluate F_{wf}. The following relationships may then be derived.

$$A_3 F_{3\ell} = A_1 F_{13} + A_2 F_{23} \tag{3.25a}$$

$$F_{wf} = F_{3\ell} = 2\left(\frac{A_1}{A_w}\right) F_{13} = \sqrt{2}\, F_{13} \tag{3.25b}$$

$$F_{12} + F_{13} = 1 \tag{3.25c}$$

$$F_{wf} = \sqrt{2}\,(1 - F_{12}) \tag{3.25d}$$

The remaining view factor introduced, F_{12}, may be calculated using a chart reprinted from Hottel in Rohsenow (15), which gives the view factor for direct radiation between adjacent rectangles in perpendicular planes. This chart is reproduced in Figure 18.

Since the radiation heat flux at the spacer must be based on the entire pipe area, the fraction of wall area seen by the spacer of

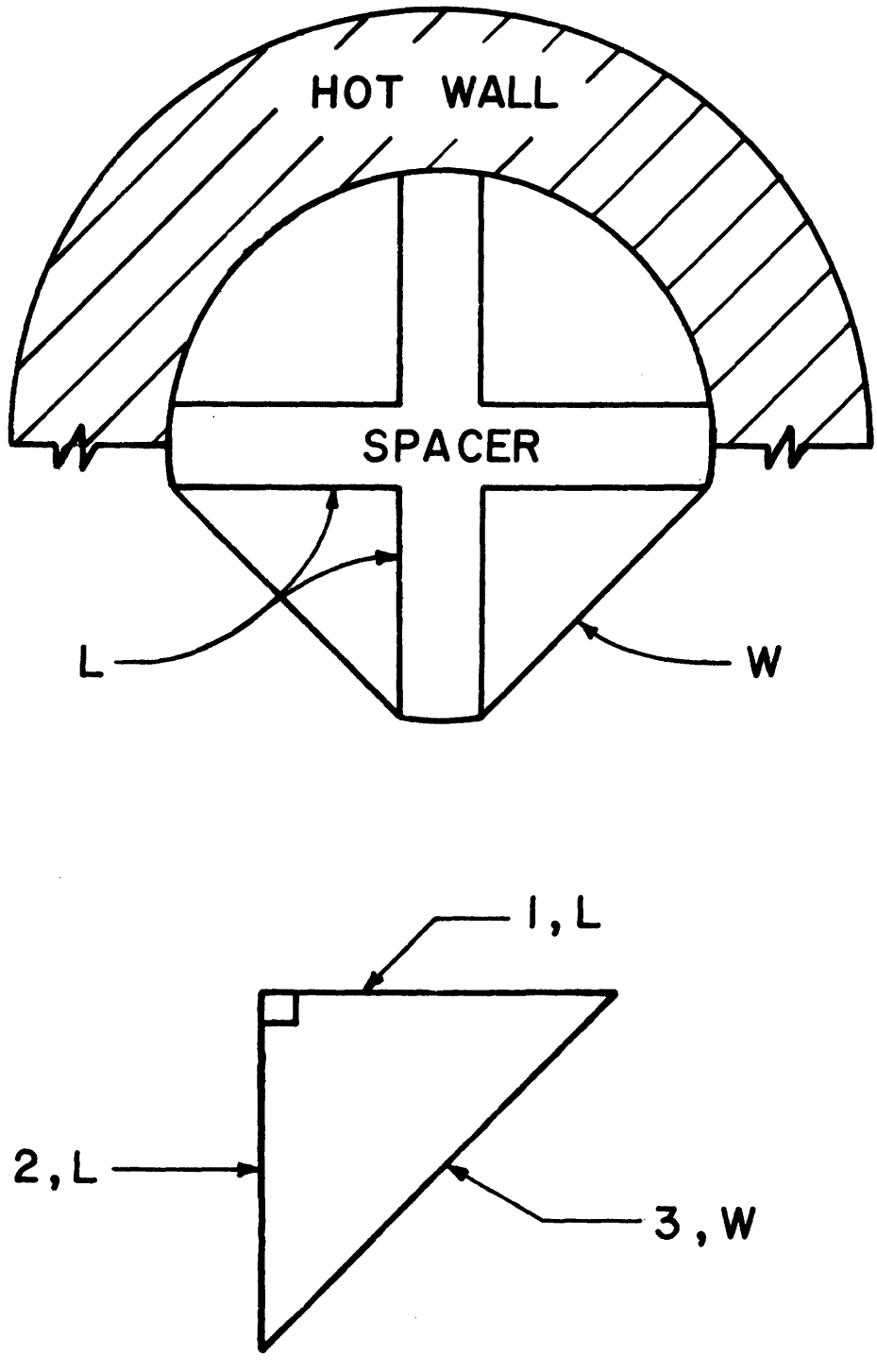

FIGURE 17: SPACER IDEALIZATION

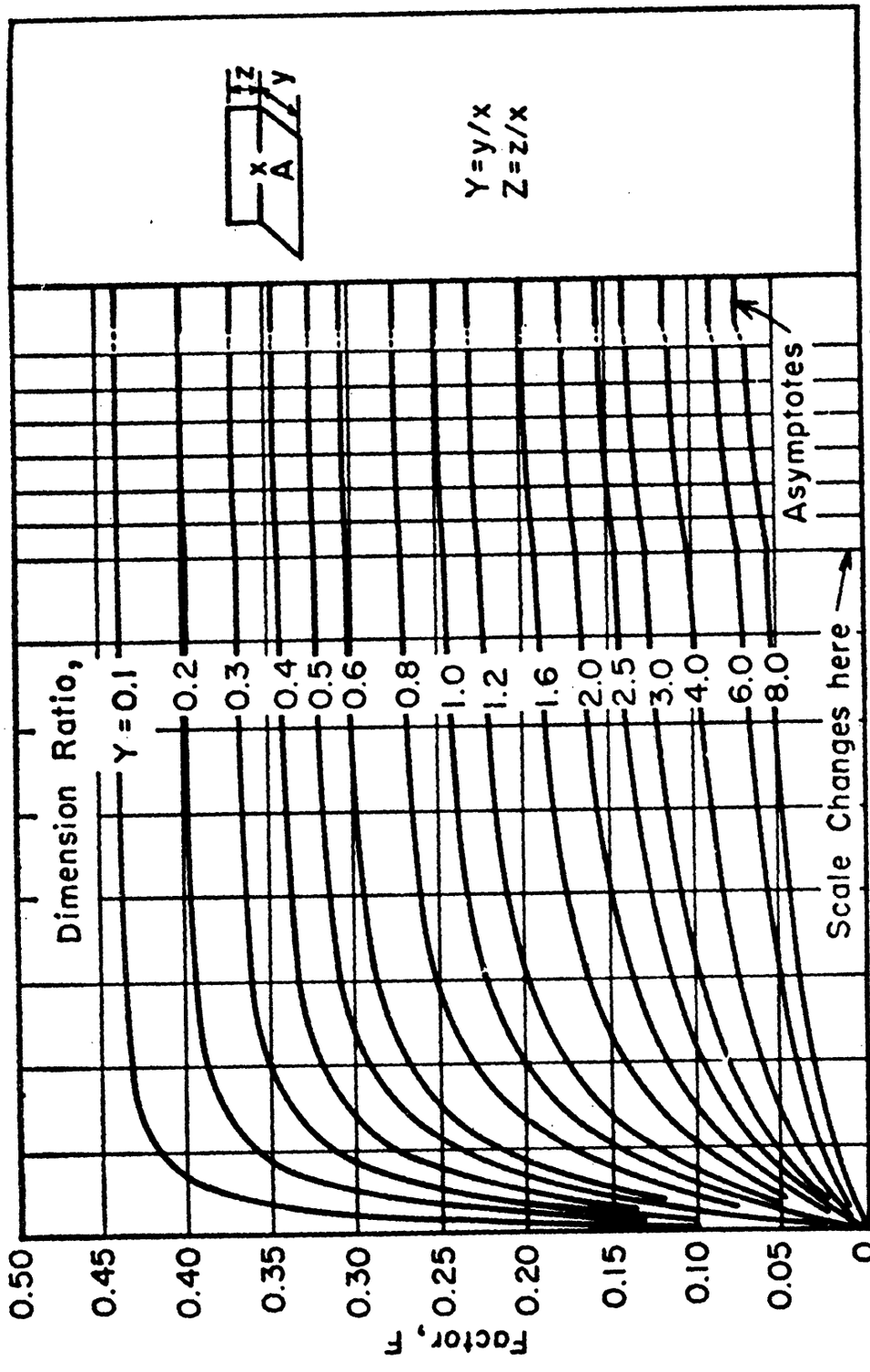

FIGURE 18: VIEW FACTOR, F, FOR DIRECT RADIATION BETWEEN ADJACENT PERPENDICULAR PLANES

the total area must be defined.

$$\beta = \frac{A_w}{A} \tag{3.26}$$

Substituting this relationship into Equation 3.22 yields an expression for the radiation heat flux experienced at the spacer.

$$(q/A)_{RS} = \beta \mathcal{F}_{wf} \sigma (T_w^4 - T_s^4) \tag{3.27}$$

In this investigation, the following values were appropriate,

$$\beta = .801 \tag{3.28a}$$

$$\varepsilon_\ell = .96 \tag{3.28b}$$

$$\varepsilon_w = .94 \tag{3.28c}$$

$$F_{12} = .29 \tag{3.28d}$$

$$F_{wf} = 1.0 \tag{3.28e}$$

Substituting into Equation 3.24 yields,

$$\mathcal{F}_{wf} = .92 \tag{3.29}$$

CHAPTER IV:

EXPERIMENTAL RESULTS AND COMPARISON TO THEORY

4.1 EXPERIMENTAL HEAT FLUX RESULTS

Tests were conducted at a mass flux of 18, 720 lbm/hr-ft^2, which is equivalent to a flooding rate of 1 in/sec. The test section wall temperatures included 1000°F, 1100°F, 1200°F and 1300°F while the system pressure was kept at atmospheric. Numerous attempts were made to obtain data at both higher flooding rates and greater Reynolds Number values (Re_v > 5000). Unfortunately, all of these efforts were thwarted by an inlet quench problem. Further comments with regard to this will be made in Chapter V. Heat flux results obtained from the successful runs are plotted along with the corresponding theoretical curves in Figures 19, 20, 21 and 22.

Several portions of these curves first deserve identification. The shaded region at the start of each plot represents the range of anticipated entrance effects as predicted by cases 2 and 3 in Figure 15. This did indeed compare reasonably well with experimental values. Flat portions of the curves indicate steady-state values which were obtained both upstream and downstream of the spacer. The effect of the spacer itself is clearly recognizable by the sudden combination of step increase and step decrease in the predicted heat flux at the 10-1/2 inch and 12 inch marks respectively. These figures strongly infer that there is a very noticeable enhancement of heat transfer experienced at the spacer location.

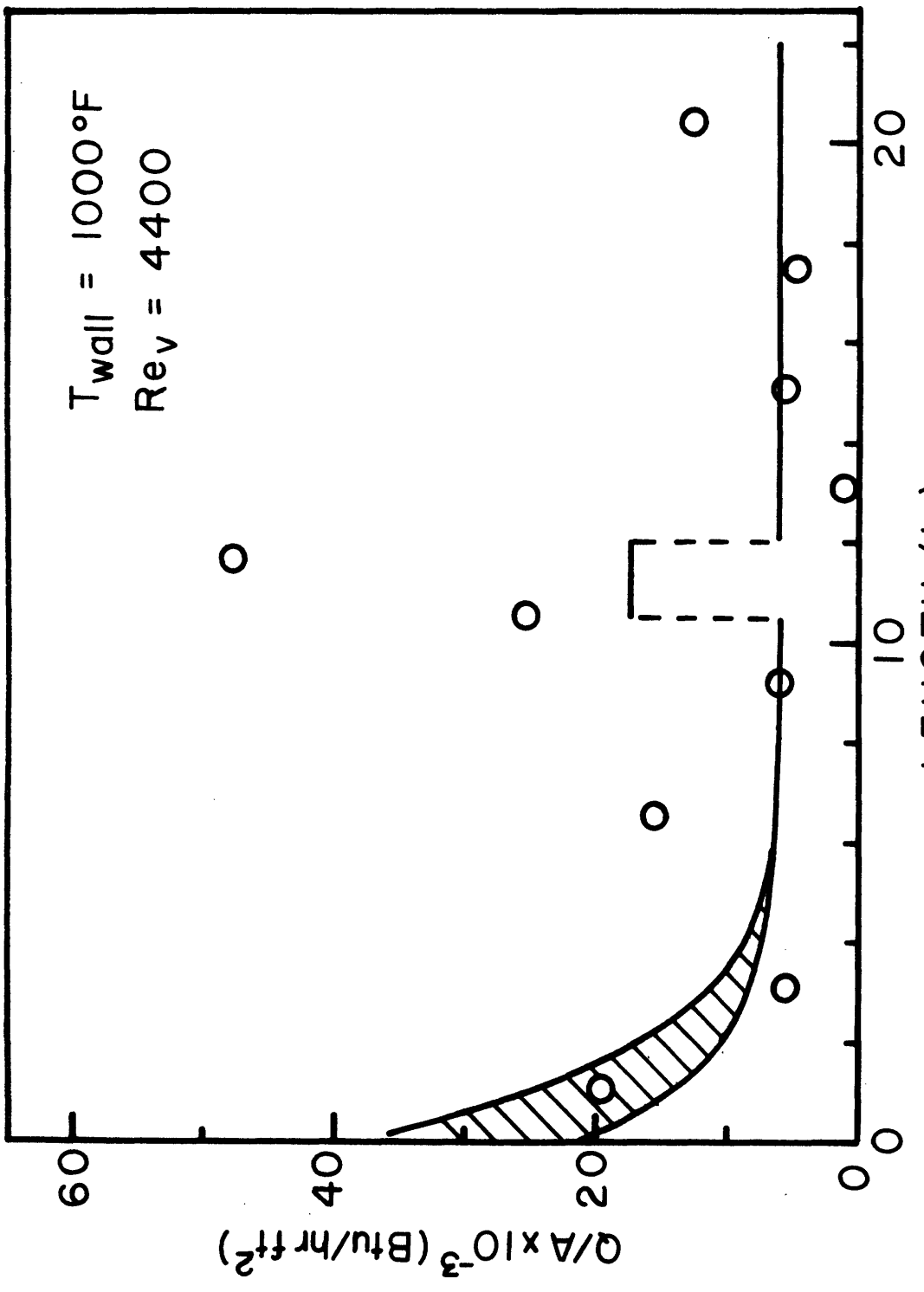

FIGURE 19: COMPARISON OF DATA AT 1 IN/SEC AND 1000°F TO THEORY

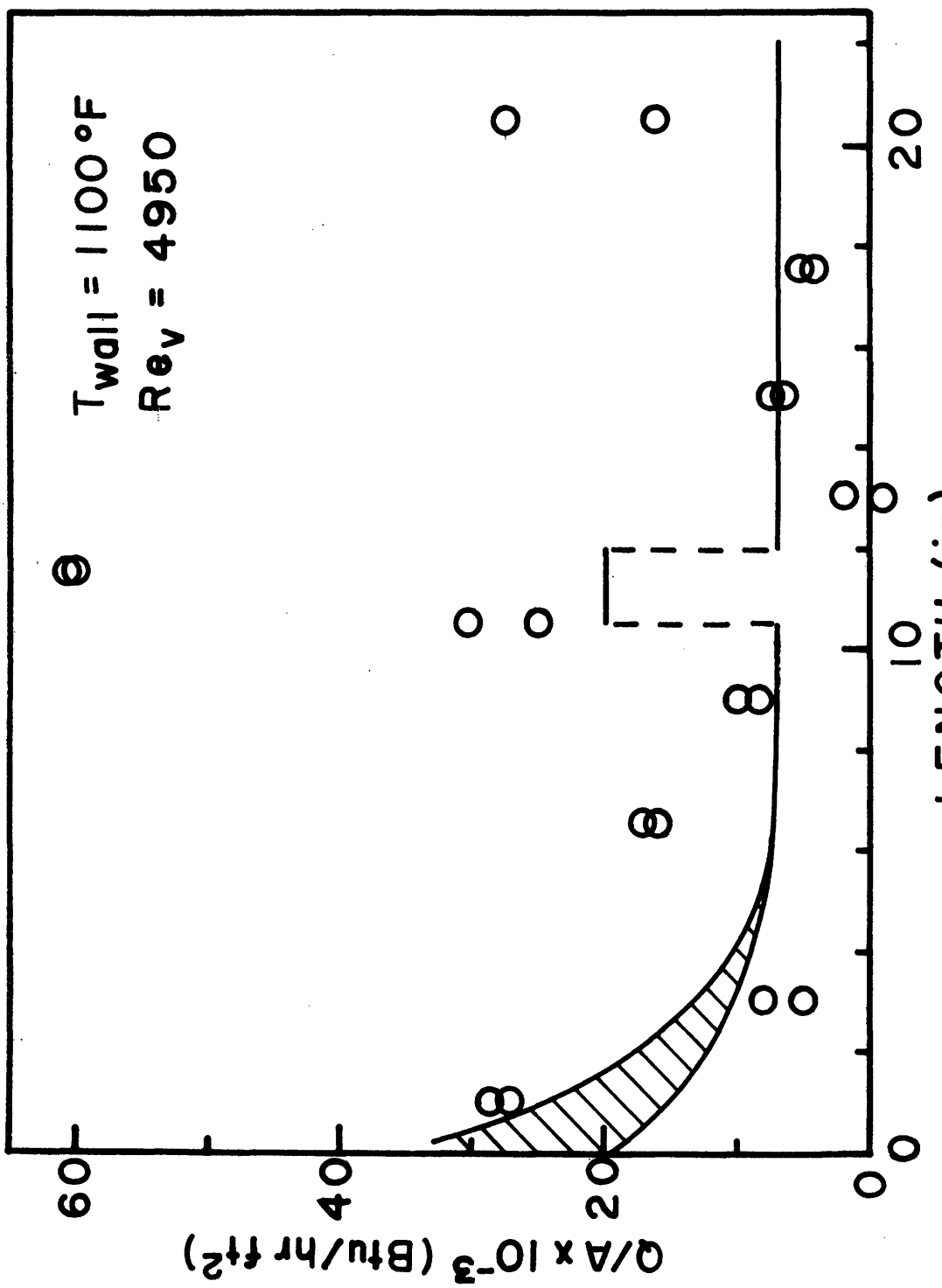

FIGURE 20: COMPARISON OF DATA AT 1 IN/SEC AND 1100°F TO THEORY

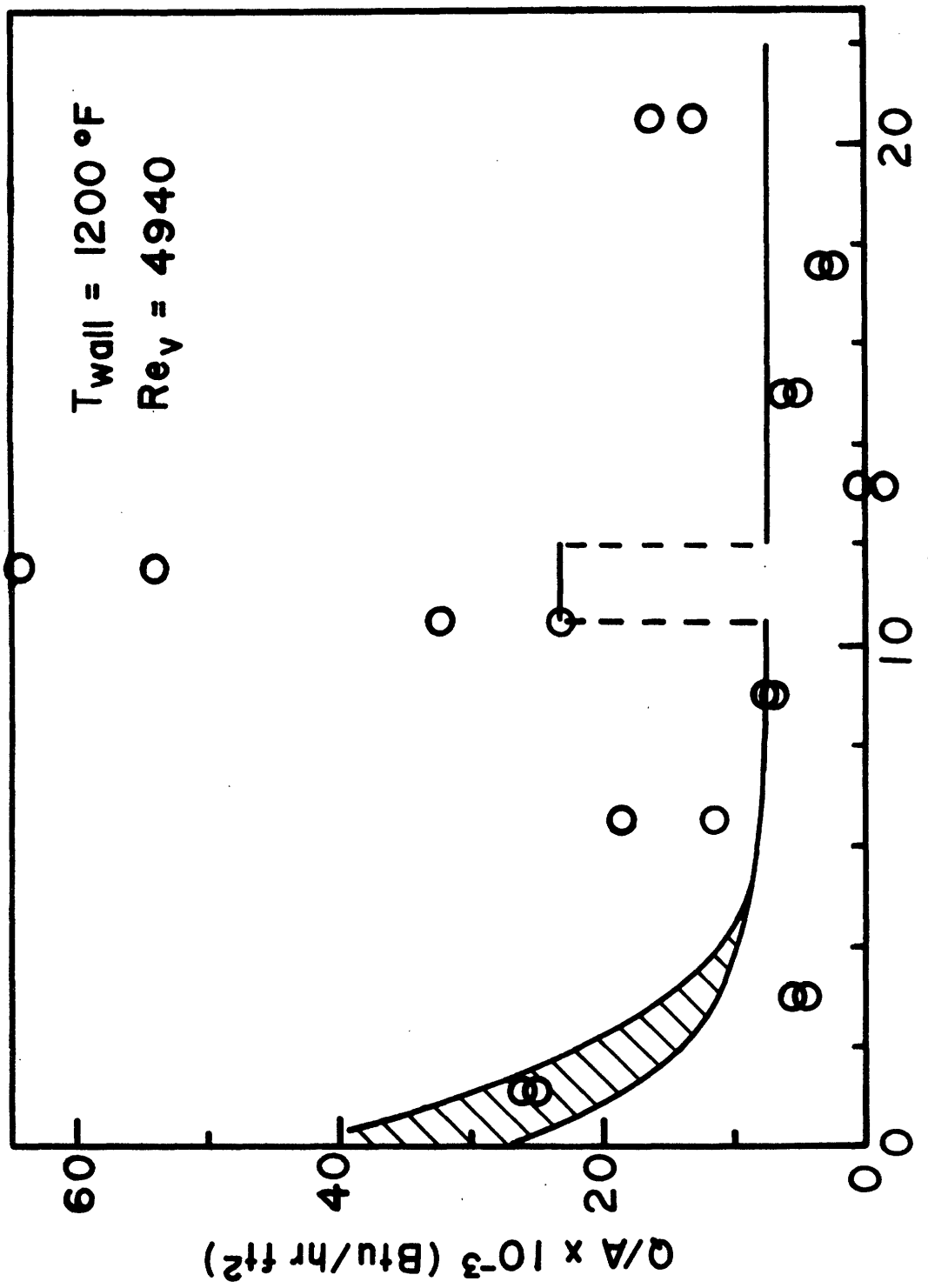

FIGURE 21: COMPARISON OF DATA AT 1 IN/SEC AND 1200°F TO THEORY

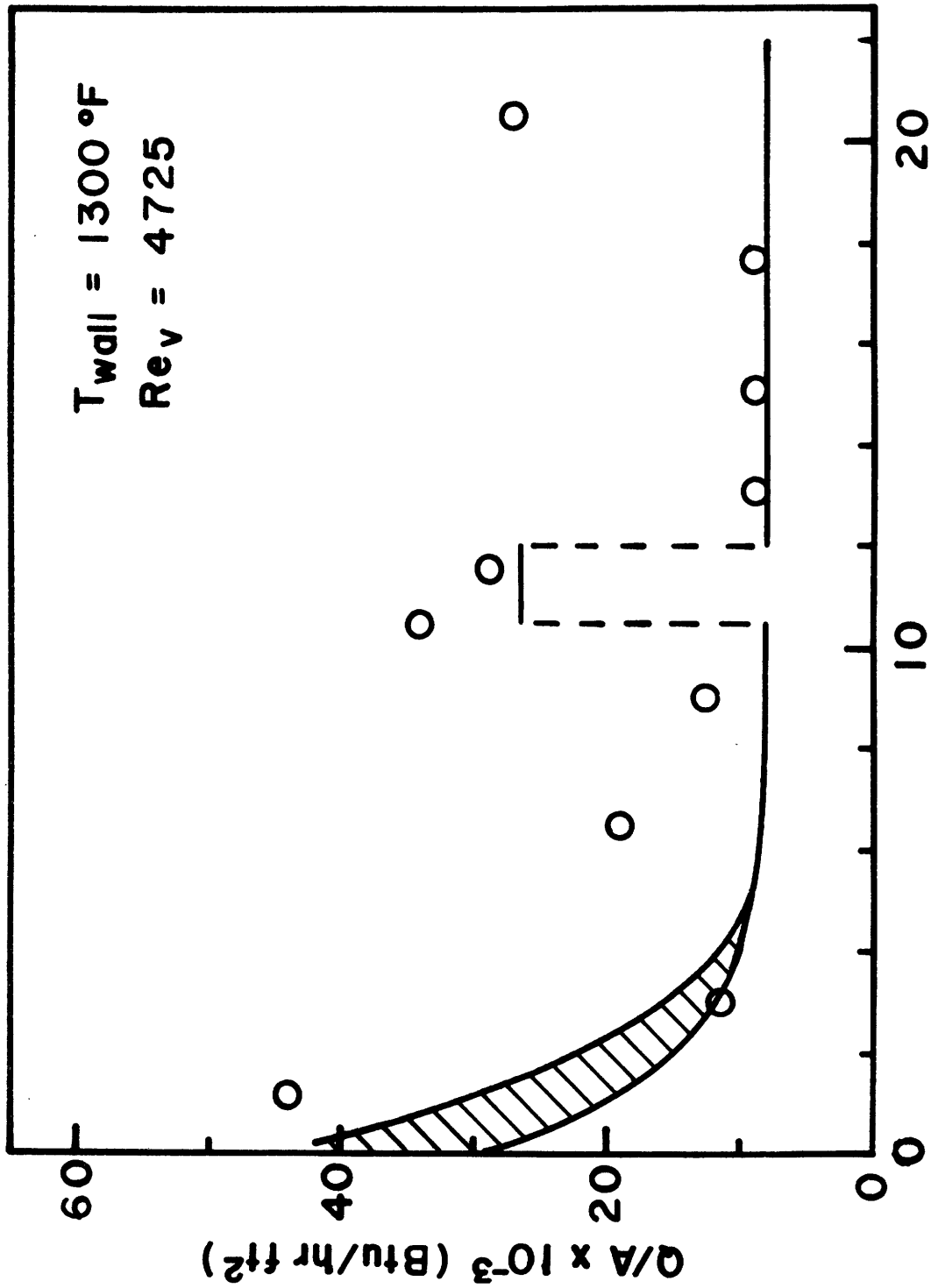

FIGURE 22: COMPARISON OF DATA AT 1 IN/SEC AND 1300°F TO THEORY

Although the experimental data straddles the theoretical model, the magnitude of its scatter is at first alarming. The major cause of this behavior is due to copper block temperature differences, creating an axial heat transfer not accounted for in the model. More specifically, the test section wall temperature is controlled to be at a constant level along its length. Heat flux spikes, however, vary significantly from block to block. This results in differences in copper block temperatures which act as the driving potentials causing the heat flux spikes. Due to this temperature variance, heat is convected across the 1/8 inch gap from one block to another. This effect is felt most strongly at the spacer where the net heat flux is considerably greater than the fully-developed value. Accordingly, heat is transferred directly to the neighboring cooler blocks. Figures 19 and 20 exemplifying this situation, both indicate a negative net heat transfer immediately downstream of the spacer. What this all indicates is simply that the experimental heat fluxes at the spacer should be decreased enough in order that the neighboring values be increased to at least the fully-developed value, such that the total energy transferred remains constant. Since the two blocks at the spacer are only one half as thick as the adjacent ones, the high experimental heat flux results obtained at the spacer should be decreased a distance equal to twice the increase in magnitude of the lower values.

The primary inpetus of this investigation is the specific determination of the spacer grid's effect. With this goal in mind, a

more detailed analysis of the effect will now be considered.

4.2 EFFECTIVE HEAT TRANSFER ADDITION AT SPACER

A local heat transfer coefficient can be determined similar to the experimental heat transfer coefficient given in Equation 2.8.

$$h_x = \frac{(q/A)_x}{(T_{wall} - T_{sat})} \tag{4.1}$$

When a flow reaches steady-state, this parameter also obtains a constant value given by h_∞. The ratio h_x to h_∞ yields a nondimensional heat transfer coefficient magnitude.

$$\frac{h_x}{h_\infty} = \frac{(q/A)_x}{(q/A)_\infty} \tag{4.2}$$

When Figures 19 through 22 are replotted in this fashion, they completely coincide except at the spacer. Figure 23 indicates that a three fold increase in the local heat transfer coefficient is experienced at this location. This effect is caused by the radiation mode of heat transfer, which is heavily dependent on temperature and is localized at the spacer.

The magnitude of increase in heat transfer caused by the spacer can also be obtained by integrating the heat flux curves. In this process, the valleys immediately before and after the high spacer heat flux values are accounted for, such that the previously ignored problem of thermal interaction between adjacent blocks is virtually eliminated. These integrated values are plotted in Figure 24 along

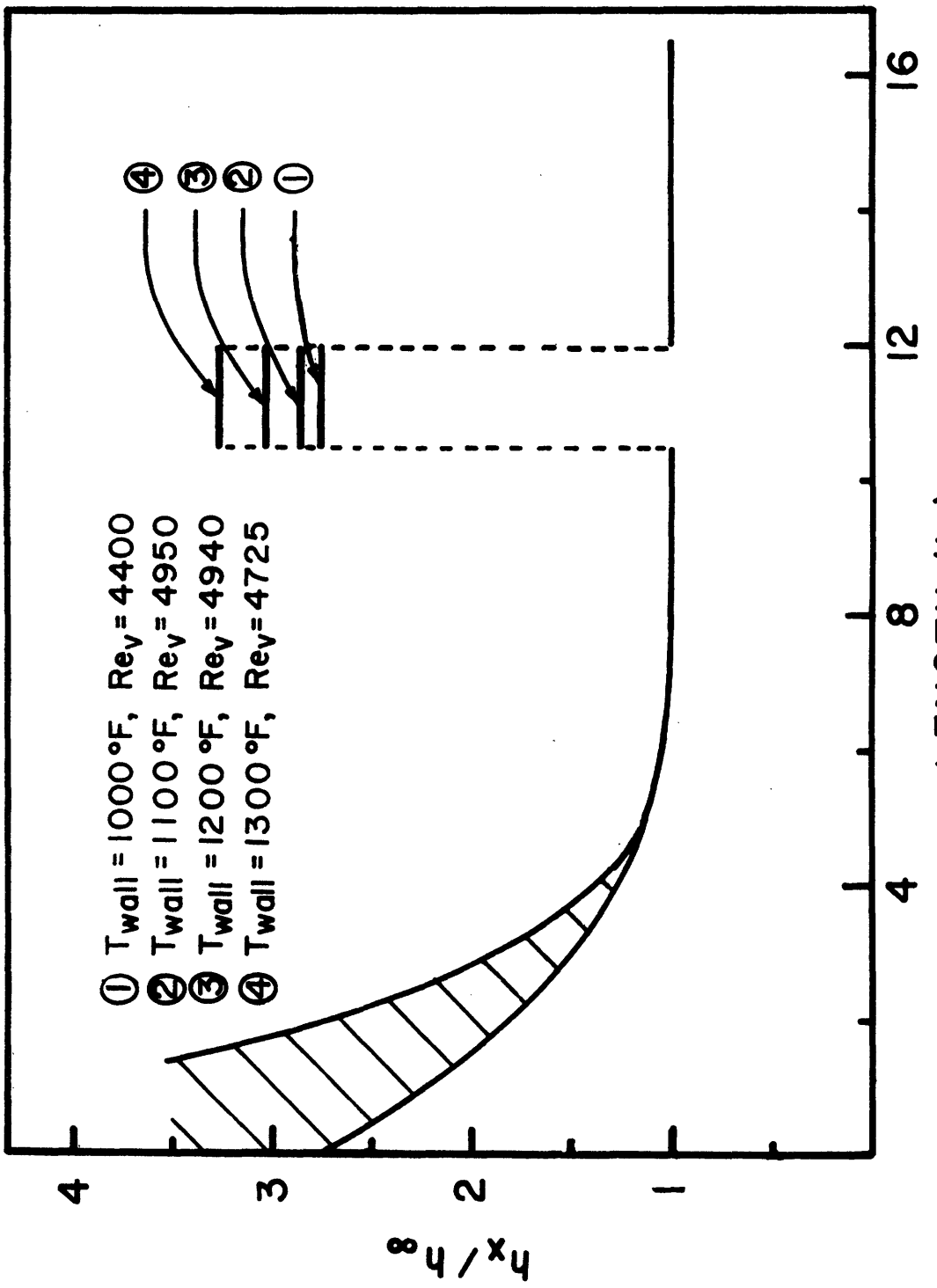

FIGURE 23: THEORETICAL NONDIMENSIONAL HEAT TRANSFER COEFFICIENT

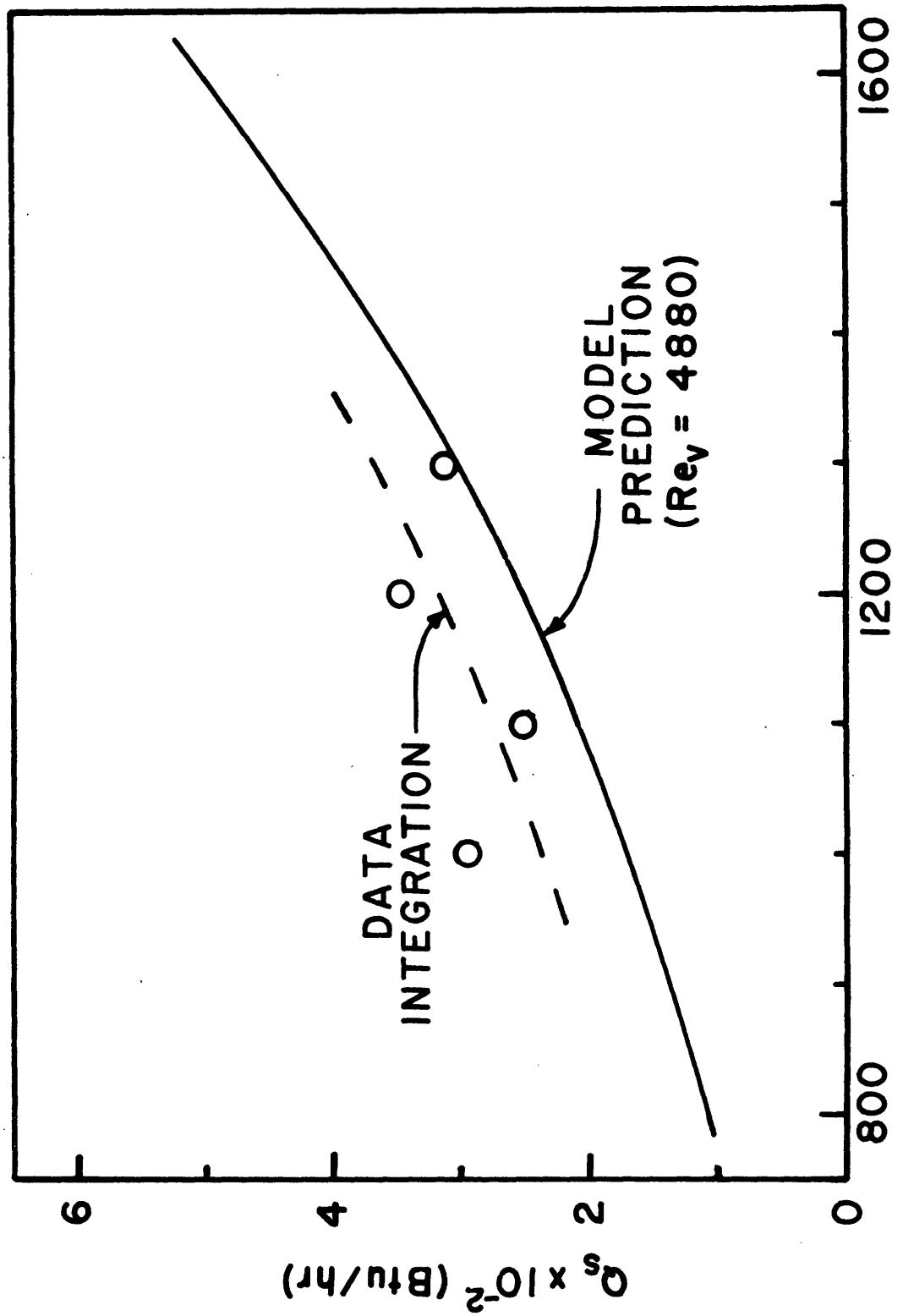

FIGURE 24: SUPPLEMENTAL HEAT TRANSFER AT SPACER

with a theoretical curve obtained from the model presented in Chapter III. Although this model underestimates the experimental findings, the correlation between the two is much better than indicated earlier by the heat flux curves. As the wall temperature increases, the model seems to predict a greater percentage of the experimentally determined spacer heat transfer. This trend is directly caused by the increasing importance of wall to spacer radiation at higher temperatures, which is easily accounted for. To make this concept clearer, the total energy transferred at the spacer, based on the theoretical model, is broken down between the three heat transfer modes by percentage and plotted in Figure 25. At lower temperatures, the radiation effect is not much greater than the droplet contribution; however, radiation becomes the primary mode of heat transfer beyond 1400°F.

Several reasons for the model's underpredictions seem plausible. A disturbance caused by the flow's constriction at the spacer may induce an entrance effect at the spacer and slightly downstream of it. This, however, would not effect the radiation contribution, and therefore is consistent with the trend illustrated in Figure 24. A second consideration is the exceptionally high temperature of copper blocks located at the spacer. Not only is heat transferred axially, but an increased radial heat loss is experienced which is greater than that measured during heat loss tests. In summary, we see that there are reasons why the actual heat transfer at the spacer is greater than what the model predicts but also less than what experimental results may have us believe.

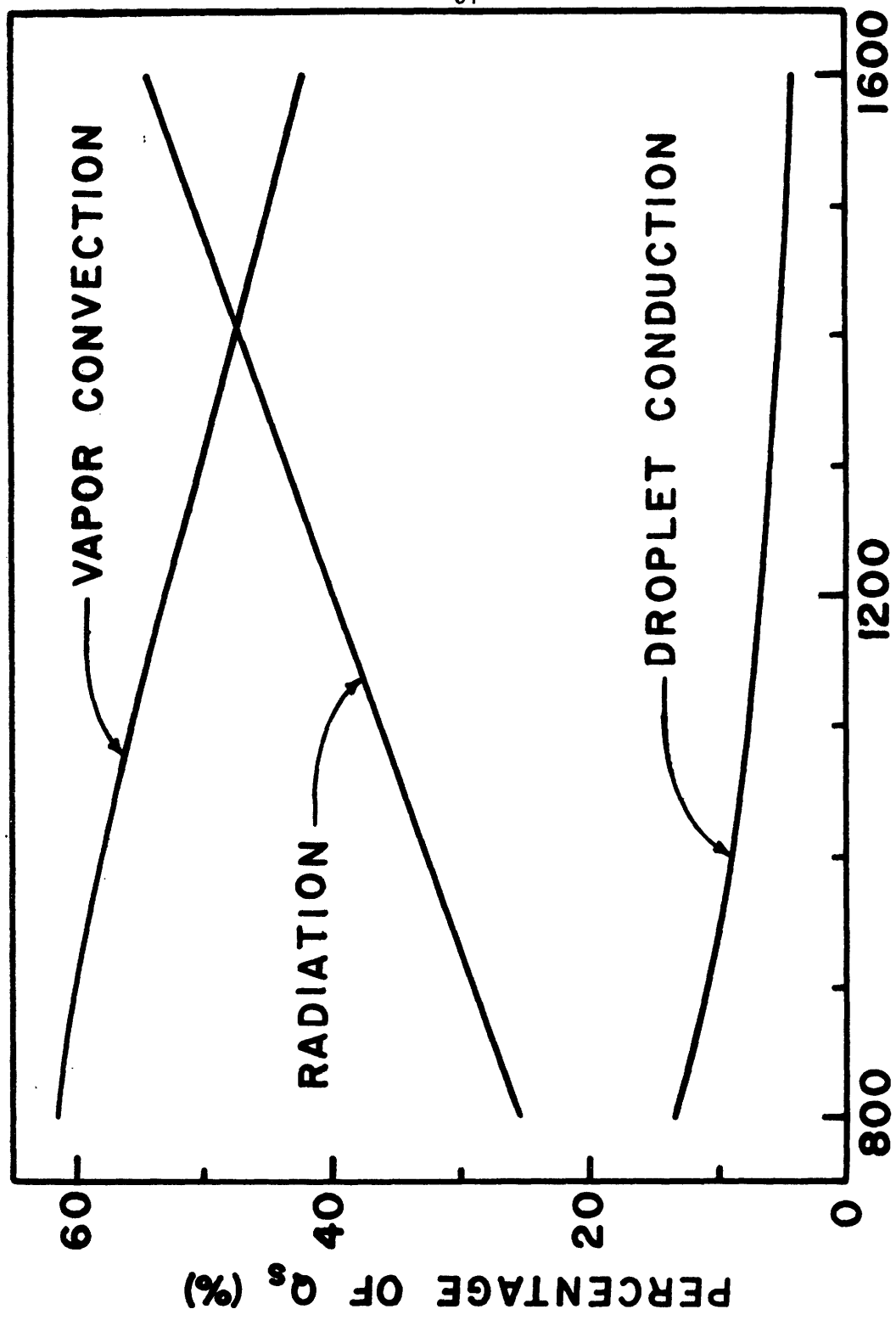

FIGURE 25: THEORETICAL BREAKDOWN OF HEAT TRANSFER AT SPACER

CHAPTER V:

CONCLUSIONS AND RECOMMENDATIONS

5.1 CONCLUSIONS

The goal of this investigation was to determine the extent of spacer induced heat transfer enhancement during a post critical heat flux situation. In this vein both experimental and theoretical programs were designed to quantitatively analyze the magnitude of this effect. Wall temperature was varied in increments of 100 degrees between 1000°F and 1300°F. The mass flux equaled 18,720 lbm/hr-ft^2, which is equivalent to a 1 in/sec flooding rate.

The "Fixed Vapor Fraction Model" predicted entrance and steady-state heat transfer levels consistent with experimental values. Where discrepancies at the spacer due to experimental scatter occurred, an integration scheme was applied which accounted for a heat transfer interaction not included in the theoretical model. Results indicate that for the flows considered, an increase of at least three times the net heat transfered at the spacer may be expected. This supplemental energy from the hot wall at the spacer is primarily due to:

(1) Higher vapor velocities which increase the vapor convection and droplet conduction.

(2) Wall to saturated liquid (entrained on the spacer) radiation.

The first effect is independent of wall temperature and depends simply on the steady-state flow. The magnitude at the spacer will be a constant multiple (with respect to temperature) of the steady-state value.

The second effect, radiation, is only dependent on wall temperature and provides extra heat transfer localized at the spacer. When the wall temperature exceeds 1400°F, the radiation effect dominated in the low Reynolds Number (Re_v = 4800), low flooding rate (1 in/sec) situation.

One final consideration concerns an entrance effect at the spacer. Similar to the initial portion of the test section, a rise in heat transfer may result from unsteady flow behavior. Assuming this to be the case, the theoretical model incorporated in this analysis will underpredict the vapor convection and droplet conduction. The radiation contribution, however, will not be affected since it is independent of the vapor flow.

5.2 RECOMMENDATIONS

Several suggestions seem in order with regard to future spacer grid analysis; in particular, construction of the experimental apparatus. In this study, thin copper heating blocks were used at the spacer in hopes of obtaining a more sensitive measurement. Since the cartridge heaters were inserted radially, a large block diameter was required. This tended to greatly aggravate the inter-block heat transfer problem, which was the primary cause of data scatter. In the future, one heating block should be employed at the spacer with a thickness of approximately two inches and all block diameters throughout the test section should be minimized. In addition, thermocouples could be mounted on the copper blocks in order to determine any remaining thermal

interaction between blocks and to more accurately account for individual block heat losses to the environment.

A second recommendation pertains to the test section inlet. Liquid leaving the electric preheater was able to wet the unheated pipe wall previous to the test section. Upon entering the heated section, the first block received full responsibility of maintaining a vapor blanket on the pipe wall. This tended to be an unstable situation since liquid constantly rewetted the start of the test section, violently pulling the wall tempeature out of the post critical heat flux region before the controller mechanism could have an effect. During downflow studies, the flow can be funneled into the test section, mechanically providing an artificial dry starting length as the flow is expanding. This cannot be applied to the upflow situation since the gravitational force would tend to form a pool of water between the funnel and test section wall. What is required is a totally different approach, one which can insure that the post CHF state of the test section inlet flow is maintained.

REFERENCES

1. Hsu, Y.Y. and Sullivan, H., "Thermal-Hydraulic Aspects of PWR Safety Research", Thermal and Hydraulic Aspects of Nuclear Reactor Safety, Vol. 1, 1977.

2. Bjørnard, T.A., "Blowdown Heat Transfer in a Pressurized Water Reactor", PH.D. Thesis, Massachusetts Institute of Technology, August 1977.

3. Smith, T.A., "Heat Transfer and Carry Over of Low Pressure Water in a Heated Vertical Tube", Masters Thesis, Massachusetts Institute of Technology, January 1976.

4. Robershotte, P., "Downflow Post Critical Heat Flux Heat Transfer of Low Pressure Water", Masters Thesis, Massachusetts Institute of Technology, July 1977.

5. Kaufman, J.M., "Post Critical Heat Flux Heat Transfer to Water in a Vertical Tube", Masters Thesis, Massachusetts Institute of Technology, September 1976.

6. Singh, B., Current Research at the Mechanical Engineering Heat Transfer Lab, Massachusetts Institute of Technology.

7. Cheung, Y., Current Research at the Mechanical Engineering Heat Transfer Lab, Massachusetts Institute of Technology.

8. Gonzalez-Rivas, J.I., "Carry-Over Predictions from the Upper Plenum of a Pressurized Water Reactor Based on a First Order Void Fraction Analysis", Masters Thesis, Massachusetts Institute of Technology, May 1978.

9. Dittus, F.W. and Boelter, L.M.K., University of California Pub. Eng. 3, 443, 1930.

10. ESDU (1968), "Forced Convective Heat Transfer in Circular Tubes", Part III: Further Data for Turbulent Flow. Item No. 68007, (251-259 Regent St., London W1R 7AD).

11. Ganić, E.N. and Rohsenow, W.M., "Post Critical Heat Flux Heat Transfer", MIT Report No. 82672-97, June 1976.

12. Liu, B.Y.H. and Ilori, T.A., "Inertial Deposition of Aerosol Particles in Turbulent Pipe Flow". Presented at the ASME Symposium on Flow Studies in Air and Water Pollution. Atlanta Georgia, 20-22 June 1973.

13. Kendall, G., "Heat Transfer to Impacting Drops and Post Critical Heat Flux Dispersed Flow", Ph.D. Thesis, Massachusetts Institute of Technology, March 1977.

14. Hottel, H.C. "Radiation", Chapter IV of Heat Transmission, by W.H. McAdams, McGraw-Hill, 1954.

15. Rohsenow, W.M. and Choi, H.Y., Heat Mass and Momentum Transfer, Prentice-Hall Inc., 1961.

APPENDIX A: TEMPERATURE CONTROLLER

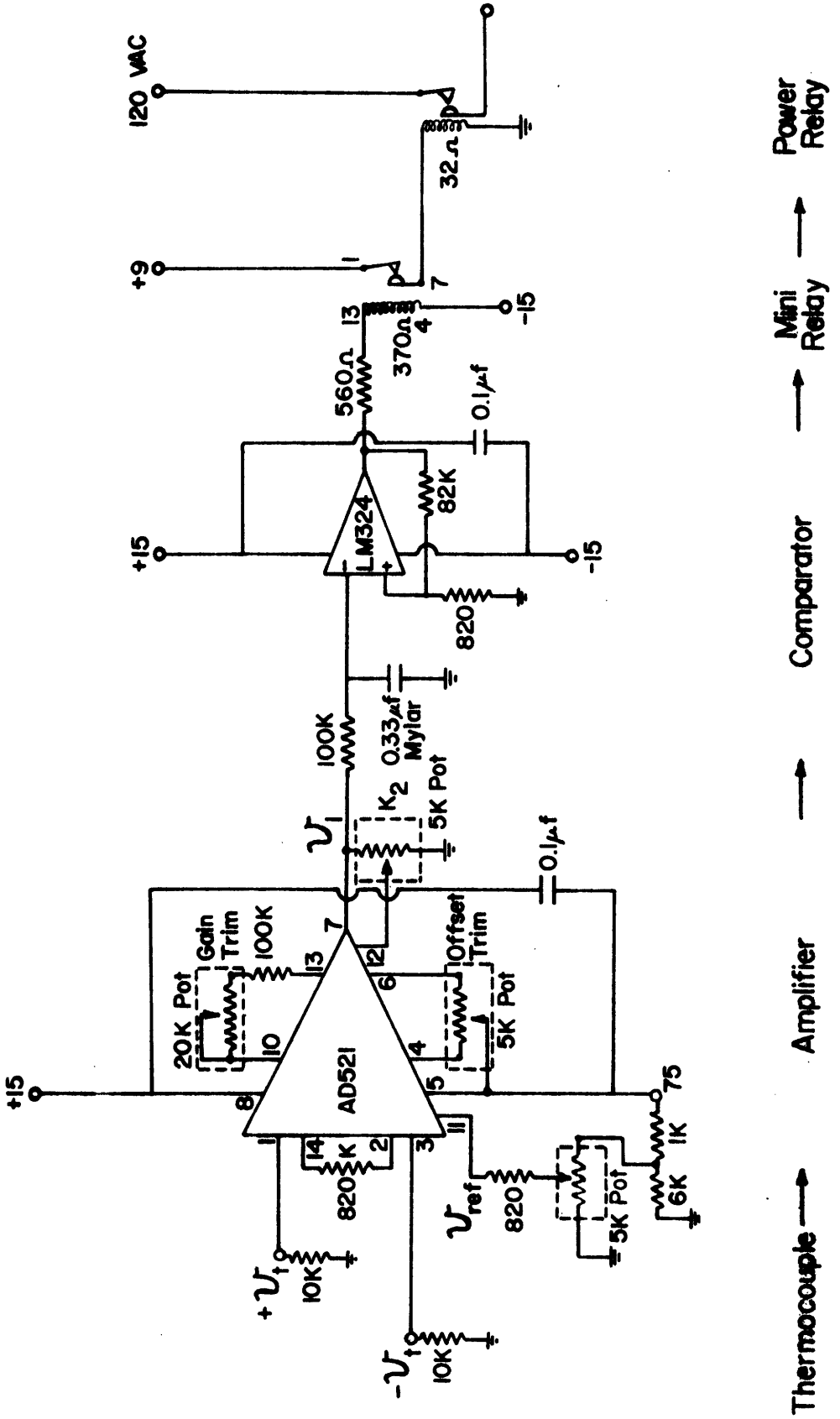

FIGURE 26. WALL TEMPERATURE CONTROLLER CIRCUIT DIAGRAM

APPENDIX B

EXPERIMENTAL DATA

RUN	T_{wall}	$(Re_v)_{inlet}$
1	1000°F	4300
2a	1100°F	4800
2b	1100°F	4950
3a	1200°F	4850
3b	1200°F	5000
4	1300°F	4725

Flow = 18,720 lbm/hr-ft^2, PRESS = 0 psig

RUN 1, FLOW = 18,720 lbm/hr-ft^2, $(Re_v)_{inlet}$ = 4300, T_{wall} = 1000°F

DIST (in)	VOLTAGE (volts)	RES (ohms)	POWER (watts)	t_{on} (min)	q_{GROSS} (Btu/hr)	$(q/A) \times 10^{-3}$ GROSS (Btu/hr-ft^2)	$(q/A) \times 10^{-3}$ NET (Btu/hr-ft^2)
1.0	80	6.54	979	5.67	949	44.04	19.42
3.5	50	4.51	554	4.5	427	13.20	5.51
6.5	45	4.51	449	9.4	721	22.30	15.91
9.0	40	8.16	196	8.2	275	12.76	5.66
10.5	70	18.7	262	8.0	358	33.28	25.93
11.5	80	20.4	313	11.7	625	58.27	48.42
13.0	50	6.70	373	2.6	166	7.70	.96
15.0	40	6.66	240	5.6	229	10.68	5.35
17.5	40	4.47	358	5.9	362	11.18	4.56
20.5	70	4.54	1079	5.5	1014	31.41	12.38

RUN 2a, FLOW = 18,720 lbm/hr-ft^2, $(Re_v)_{inlet}$ = 4800, T_{wall} = 1100°F

DIST (in)	VOLTAGE (volts)	RES (ohms)	POWER (watts)	t_{on} (min)	q_{GROSS} (Btu/hr)	$(q/A) \times 10^{-3}$ GROSS (Btu/hr-ft^2)	$(q/A) \times 10^{-3}$ NET (Btu/hr-ft^2)
1.0	80	6.88	930	5.9	937	43.56	26.85
3.5	50	4.88	512	5.0	437	13.55	5.39
6.5	50	4.90	510	8.5	741	12.95	16.40
9.0	50	8.37	300	6.3	321	14.94	8.39
10.5	80	18.6	344	7.0	411	38.24	30.97
11.5	90	20.8	389	11.2	745	69.24	59.94
13.0	40	7.07	226	5.4	209	9.70	1.94
15.0	40	7.07	226	7.3	282	13.11	5.73
17.5	40	4.79	334	7.2	410	12.73	5.23
20.5	60	4.87	739	7.0	883	27.38	16.93

RUN 2b, FLOW = 18,720 lbm/hr-ft^2, $(Re_v)_{inlet}$ = 4950, T_{wall} = 1100°F

DIST (in)	VOLTAGE (volts)	RES (ohms)	POWER (watts)	t_{on} (min)	q_{GROSS} (Btu/hr)	$(q/A) \times 10^{-3}$ GROSS (Btu/hr-ft^2)	$(q/A) \times 10^{-3}$ NET (Btu/hr-ft^2)
1.0	70	6.88	712	8.0	973	45.23	28.52
3.5	45	4.88	415	7.0	496	15.37	7.21
6.5	45	4.90	413	10.8	762	23.62	17.07
9.0	45	8.37	242	8.7	359	16.71	9.88
10.5	70	18.6	263	7.7	346	32.20	24.93
11.5	90	20.8	389	11.6	771	71.71	62.41
13.0	35	7.07	173	4.3	127	5.91	-1.85
15.0	35	7.07	173	9.6	284	13.20	5.82
17.5	35	4.79	256	8.6	376	11.64	4.14
20.5	50	4.87	513	14.3	1253	38.85	28.40

RUN 3a, FLOW = 18,720 lbm/hr-ft^2, $(Re_v)_{inlet}$ = 4850, T_{wall} = 1200°F

DIST (in)	VOLTAGE (volts)	RES (ohms)	POWER (watts)	t_{on} (min)	q_{GROSS} (Btu/hr)	$(q/A) \times 10^{-3}$ GROSS (Btu/hr-ft^2)	$(q/A) \times 10^{-3}$ NET (Btu/hr-ft^2)
1.0	90	9.33	868	5.5	815	37.90	25.04
3.5	70	7.30	671	3.3	378	11.72	5.34
6.5	70	7.37	665	4.7	534	24.80	18.50
9.0	60	11.39	316	5.3	286	13.30	6.89
10.5	80	20.95	306	6.5	339	31.52	23.02
11.5	100	23.4	427	11.3	824	76.66	65.33
13.0	50	9.63	260	2.3	102	4.74	-1.84
15.0	50	9.66	259	5.7	252	11.71	4.83
17.5	50	7.45	336	5.3	304	9.41	1.52
20.5	80	7.41	864	5.1	752	23.31	15.82

RUN 3b, FLOW = 18,720 lbm/hr-ft^2, $(Re_v)_{inlet}$ = 5000, T_{wall} = 1200°F

DIST (in)	VOLTAGE (volts)	RES (ohms)	POWER (watts)	t_{on} (min)	q_{GROSS} (Btu/hr)	$(q/A) \times 10^{-3}$ GROSS (Btu/hr-ft^2)	$(q/A) \times 10^{-3}$ NET (Btu/hr-ft^2)
1.0	90	9.33	868	5.6	830	38.59	25.73
3.5	60	7.30	493	4.1	345	10.70	4.32
6.5	60	7.37	488	6.8	567	17.58	11.28
9.0	55	11.39	266	6.5	295	13.70	7.29
10.5	75	20.95	269	9.6	440	40.92	32.42
11.5	110	33.89	357	11.5	701	65.18	53.85
13.0	40	9.63	166	5.1	144	6.73	.15
15.0	40	9.66	166	9.6	272	12.62	5.74
17.5	40	7.45	215	9.2	337	10.46	2.63
20.5	70	7.41	661	6.1	689	21.35	13.86

RUN 4, FLOW = 18,720 lbm/hr-ft^2, $(Re_v)_{inlet}$ = 4725, T_{wall} = 1300°F

DIST (in)	VOLTAGE (volts)	RES (ohms)	POWER (watts)	t_{on} (min)	q_{GROSS} (Btu/hr)	$(q/A) \times 10^{-3}$ GROSS (Btu/hr-ft^2)	$(q/A) \times 10^{-3}$ NET (Btu/hr-ft^2)
1.0	90	6.71	1207	6.75	1391	64.7	44.0
3.5	65	4.60	919	5.0	784	24.3	12.0
6.5	65	4.75	889	6.7	1018	31.4	19.0
9.0	65	7.89	536	6.0	549	25.4	13.0
10.5	90	15.9	509	5.5	478	44.5	34.0
11.5	90	15.3	529	4.6	416	38.6	29.0
13.0	65	7.24	584	4.6	458	21.3	9.0
15.0	65	6.77	624	4.0	426	19.8	9.0
17.5	65	4.54	931	4.1	652	20.2	9.0
20.5	70	4.60	1761	4.5	1353	41.9	27.0

APPENDIX C

THEORETICAL ANALYSIS

COMPUTER PROGRAM

```
// FOR
C  POST CRITICAL HEAT FLUX HEAT TRANSFER IN A VERTICAL TUBE WITH
C  SPACER GRID EFFECTS
C
C  THEORETICAL ANALYSIS PROGRAM
C
      REAL K, MDOT, PRESS
      INTEGER TOTAL, RUN, ENTR
      DIMENSION ENT(3, 50)
C
C  CONSTANTS
C
      D = .04108333
      DSPAC = .01317
      AREA = .001325627
      ASPAC = .0008395
      A = .01075559
      CP = .48
      PR = .7
      DENL = 60.
      E = .004
      SIGMA = .1713/10.**8
      F = .92
C
C  ENTRANCE EFFECTS
C
      DO 8 KK = 1,  3, 1
      DO 6 LL = 1, 50, 1
      ENT(KK, LL) = 1.0
    6 CONTINUE
    8 CONTINUE
      ENT(1, 1) = 1.5
      ENT(1, 2) = 1.3
```

```
ENT(1, 3) = 1.2
ENT(1, 4) = 1.14
ENT(1, 5) = 1.10
ENT(1, 6) = 1.065
ENT(1, 7) = 1.04
ENT(1, 8) = 1.02
ENT(1, 9) = 1.01
ENT(2, 1) = 2.50
ENT(2, 2) = 2.66
ENT(2, 3) = 2.12
ENT(2, 4) = 1.86
ENT(2, 5) = 1.62
ENT(2, 6) = 1.48
ENT(2, 7) = 1.35
ENT(2, 8) = 1.27
ENT(2, 9) = 1.21
ENT(2,10) = 1.15
ENT(2,11) = 1.10
ENT(2,12) = 1.06
ENT(2,13) = 1.03
ENT(2,14) = 1.01
ENT(3, 1) = 2.5
ENT(3, 2) = 3.8
ENT(3, 3) = 4.1
ENT(3, 4) = 3.5
ENT(3, 5) = 2.5
ENT(3, 6) = 1.9
ENT(3, 7) = 1.6
ENT(3, 8) = 1.4
ENT(3, 9) = 1.3
ENT(3,10) = 1.2
ENT(3,11) = 1.13
ENT(3,12) = 1.07
```

```
      ENT(3,13) = 1.03
C
C   INPUT FIRST DATA CARD
C
      READ(8, 10) TOTAL, ENTR
   10 FORMAT(2I3)
C
C   PRINT OUTPUT HEADING
C
      WRITE(5, 20) TOTAL
   20 FORMAT('0', 20X, 'THEORETICAL ANALYSIS OF', I3, ' EXPERIMENTAL RUN
     2(S)')
C
C   LOOP OVER EACH RUN
C
      DO 800 N = 1, TOTAL, 1
C
C   INPUT DATA CORRESPONDING TO EACH RUN
C
      READ(8, 30) RUN, TWALL, TSAT, PRESS, HFG, G, REIN, X
   30 FORMAT(I3, F17.1, 5F10.1, F10.4)
      MDOT = G*A
      TRAD = (TWALL + 460.)**4 - (TSAT + 460.)**4
C
C   PRINT OUTPUT HEADING FOR EACH RUN
C
      WRITE(5, 40) RUN, TWALL, TSAT, PRESS, G, X, REIN
   40 FORMAT('1', 10X, 'RUN',I3, ',  TWALL=', F5.0, '  TSAT=', F4.0,
     2'  PRESS=', F3.0, '  GFLUX=', F7.0, '  XEQ=', F6.4, '  (RF)INLET='
     3, F7.0)
      WRITE(5, 50)
   50 FORMAT('0', 12X, 'DISTANCE', 6X, 'EQUILIBRIUM', 6X, 'REYNOLDS',
     29X, 'HEAT', 7X, 'HEAT TRANSFER', 7X, 'VAPOR')
```

```
      WRITE(5, 60)
   60 FORMAT(' ', 28X, 'QUALITY', 9X, 'NUMBER', 10X, 'FLUX', 8X,
     2'COEFFICIENT', 5X, 'TEMPERATURE')
C
C  LOOP OVER EACH ENTRANCE EFFECT AND PRINT OUTPUT HEADING
C
      DO 300 IENT = 2, ENTR, 1
      WRITE(5, 100) IENT
  100 FORMAT('0', 35X, 'RESULTS USING ENTRANCE EFFECT CASE', I2)
C
C  INITIALIZE VARIABLES
C
      XEQ = X
      XIN = X
      TVAP = TSAT
      TIN = TSAT
C
C  COMPUTATION OF HEAT FLUX ALONG TEST SECTION BEFORE THE SPACER
C
      DO 250 I = 1, 21, 1
      DIST = .5*FLOAT(I)
  140 K = .000032*TVAP + .00690
      VIS = .0000551*TVAP + .01747
      DENV = .04559 - .00003958*TVAP
C
C  WALL TO VAPOR HEAT TRANSFER
C
      RE = XEQ*G*D/VIS
      PR = CP*VIS/K
      HDB = ENT(IENT, I)*.023*K*(RE**.8)*(PR**.4)/D
      QV = HDB*A*(TWALL - TVAP)
      VV = G*XEQ/DENV
      VD = VV/100.
```

```
      XX = (1. + XEQ)/XEQ
      DD = DENV/DENL
      ALPHA = 1./(1. + XX*DD)
C
C  WALL TO DROPLET HEAT TRANSFER
C
      QD = (1. - ALPHA)*DENL*HFG*VD*E*A
C
C  TOTAL HEAT TRANSFER
C
      QT = QV + QD
      TOUT = TIN + QT/(X*MDOT*CP)
      XOUT = XIN + QT/(MDOT*HFG)
      TNEW = (TOUT + TIN)/2.
      XNEW = (XOUT + XIN)/2.
      TDIFF = TNEW - TVAP
      DIFF = ABS(TDIFF)
      TVAP = TNEW
      XEQ = XNEW
      IF (DIFF .GE. .01) GO TO 140
      QFLUX = QT/A
      H = QFLUX/(TWALL - TSAT)
C
C  PRINT THEORETICAL RESULTS
C
      WRITE(5, 180) DIST, XEQ, RE, QFLUX, H, TVAP
  180 FORMAT(' ', F18.2, F16.4, F15.0, F16.0, F15.2, F16.1)
C
C  REINITIALIZE VARIABLES FOR NEXT ELEMENT
C
      TIN = TVAP
      TVAP = TOUT
      XIN = XEQ
```

```
      XEQ = XOUT
  250 CONTINUE
  300 CONTINUE
C
C   BEGIN ANALYSIS FOR TEST SECTION AT THE SPACER
C
      GSPAC = G*AREA/ASPAC
      DO 500 I = 22, 24, 1
      DIST = .5*FLOAT(I)
  340 K = .000032*TVAP + .00690
      VIS = .0000551*TVAP + .01747
      DENV = .04559 - .00003958*TVAP
C
C   WALL TO (INCREASED VELOCITY) VAPOR HEAT TRANSFER
C
      RE = XEQ*GSPAC*DSPAC/VIS
      PR = CP*VIS/K
      HDB = .023*K*(RE**.8)*(PR**.4)/DSPAC
      QV = HDB*A*(TWALL - TVAP)
C
C   WALL TO (INCREASED VELOCITY) DROPLET HEAT TRANSFER
C
      VV = GSPAC*XEQ/DENV
      VD = .0289*VV/RE**.125
      XX = (1. + XEQ)/XEQ
      DD = DENV/DENL
      ALPHA = 1./(1. + XX*DD)
      QD = (1. - ALPHA)*DENL*HFG*VD*E*A
C
C   WALL TO SATURATED LIQUID (ON SPACER) RADIATION
C
      QR = F*SIGMA*TRAD*A*.801
C
```

```
C  TOTAL HEAT TRANSFER AT SPACER
C
      QT = QV + QD + QR
      TOUT = TIN + QT/(X*MDOT*CP)
      XOUT = XIN + QT/(MDOT*HFG)
      TNEW = (TOUT + TIN)/2.
      XNEW = (XOUT + XIN)/2.
      TDIFF = TNEW - TVAP
      DIFF = ABS(TDIFF)
      TVAP = TNEW
      XEQ = XNEW
      IF (DIFF .GE. .01) GO TO 340
      QFLUX = QT/A
      H = QFLUX/(TWALL - TSAT)
C
C  WRITE THEORETICAL RESULTS AT SPACER
C
      WRITE (5, 180) DIST, XEQ, RE, QFLUX, H, TVAP
      QVFL = QV/A
      QDFL = QD/A
      QRFL = QR/A
C
C  REINITIALIZE VARIABLES FOR NEXT ELEMENT
C
      TIN = TVAP
      TVAP = TOUT
      XIN = XEQ
      XEQ = XOUT
  500 CONTINUE
C
C  COMPUTATION OF HEAT FLUX ALONG TEST SECTION DOWNSTREAM OF SPACER
C
      DO 700 I = 25, 45, 1
```

```
      DIST = .5*FLOAT(I)
  540 K = .000032*TVAP + .00690
      VIS = .0000551*TVAP + .01747
      DENV = .04559 - .00003958*TVAP
C
C   WALL TO VAPOR HEAT TRANSFER
C
      RE = XEQ*G*D/VIS
      PR = CP*VIS/K
      HDB = ENT(IENT, I)*.023*K*(RE**.8)*(PR**.4)/D
      QV = HDB*A*(TWALL - TVAP)
      VV = G*XEQ/DENV
      VD = VV/100.
      XX = (1. + XEQ)/XEQ
      DD = DENV/DENL
      ALPHA = 1./(1. + XX*DD)
C
C   WALL TO DROPLET HEAT TRANSFER
C
      QD = (1. - ALPHA)*DENL*HFG*VD*E*A
C
C   TOTAL HEAT TRANSFER
C
      QT = QV + QD
      TOUT = TIN + QT/(X*MDOT*CP)
      XOUT = XIN + QT/(MDOT*HFG)
      TNEW = (TOUT + TIN)/2.
      XNEW = (XOUT + XIN)/2.
      TDIFF = TNEW - TVAP
      DIFF = ABS(TDIFF)
      TVAP = TNEW
      XEQ = XNEW
      IF (DIFF .GE. .01) GO TO 540
```

```
      QFLUX = QT/A
      H = QFLUX/(TWALL - TSAT)
C
C  PRINT THEORETICAL RESULTS
C
      WRITE(5, 180) DIST, XEQ, RE, QFLUX, H, TVAP
C
C  REINITIALIZE VARIABLES FOR NEXT ELEMENT
C
      TIN = TVAP
      TVAP = TOUT
      XIN = XEQ
      XEQ = XOUT
  700 CONTINUE
  800 CONTINUE
      WRITE(5, 990)
  990 FORMAT('1')
      STOP
      END
// XEQ
```

APPENDIX D

THEORETICAL RESULTS

RUN	T_{wall}	$(Re_v)_{inlet}$
1	1000°F	4400
2	1100°F	4950
3	1200°F	4940
4	1300°F	4725

FLOW = 18,720 lbm/hr-ft^2, PRESS = 0 psig

RUN 1, TWALL=1000. TSAT=212. PRESS= 0. GFLUX= 18720. XEQ=0.1680 (RE)INLET= 4400.

DISTANCE	EQUILIBRIUM QUALITY	REYNOLDS NUMBER	HEAT FLUX	HEAT TRANSFER COEFFICIENT	VAPOR TEMPERATURE
		RESULTS USING ENTRANCE EFFECT CASE 2			
0.50	0.1684	4405.	13419.	17.03	216.4
1.00	0.1689	4377.	14208.	18.03	221.2
1.50	0.1691	4354.	11485.	14.57	225.0
2.00	0.1694	4334.	10172.	12.91	228.3
2.50	0.1696	4317.	8961.	11.37	231.3
3.00	0.1698	4301.	8254.	10.47	234.0
3.50	0.1700	4287.	7598.	9.64	236.5
4.00	0.1702	4274.	7194.	9.13	238.9
4.50	0.1704	4261.	6889.	8.74	241.2
5.00	0.1706	4249.	6586.	8.36	243.4
5.50	0.1708	4237.	6332.	8.04	245.5
6.00	0.1710	4226.	6129.	7.78	247.5
6.50	0.1711	4216.	5976.	7.58	249.5
7.00	0.1713	4205.	5873.	7.45	251.4
7.50	0.1714	4195.	5820.	7.39	253.4
8.00	0.1716	4185.	5817.	7.38	255.3
8.50	0.1718	4175.	5813.	7.38	257.2
9.00	0.1719	4165.	5810.	7.37	259.1
9.50	0.1721	4155.	5806.	7.37	261.1
10.00	0.1722	4145.	5802.	7.36	263.0
10.50	0.1724	4135.	5799.	7.36	264.9
		RESULTS USING ENTRANCE EFFECT CASE 3			
0.50	0.1684	4405.	13419.	17.03	216.4
1.00	0.1689	4365.	19926.	25.29	223.0
1.50	0.1695	4324.	21392.	27.15	229.1
2.00	0.1700	4289.	18353.	23.29	236.2
2.50	0.1704	4264.	13334.	16.92	240.6
3.00	0.1707	4245.	10326.	13.10	244.0
3.50	0.1709	4229.	8822.	11.20	247.0
4.00	0.1711	4215.	7819.	9.92	249.6

4.50	0.1713	4202.	7315.	9.28	252.0
5.00	0.1715	4190.	6813.	8.65	254.2
5.50	0.1717	4179.	6460.	8.20	256.4
6.00	0.1719	4168.	6158.	7.82	258.4
6.50	0.1720	4158.	5956.	7.56	260.4
7.00	0.1722	4148.	5803.	7.36	262.3
7.50	0.1723	4138.	5800.	7.36	264.2
8.00	0.1725	4128.	5796.	7.36	266.2
8.50	0.1727	4119.	5792.	7.35	268.1
9.00	0.1728	4109.	5788.	7.35	270.0
9.50	0.1730	4099.	5784.	7.34	271.9
10.00	0.1731	4090.	5780.	7.34	273.8
10.50	0.1733	4080.	5776.	7.33	275.7
11.00	0.1737	2053.	15866.	20.13	281.0
11.50	0.1742	2040.	15845.	20.11	286.2
12.00	0.1746	2027.	15824.	20.08	291.5
12.50	0.1748	3996.	5735.	7.28	293.4
13.00	0.1749	3987.	5731.	7.27	295.3
13.50	0.1751	3979.	5726.	7.27	297.2
14.00	0.1752	3970.	5722.	7.26	299.1
14.50	0.1754	3961.	5717.	7.25	301.0
15.00	0.1756	3953.	5712.	7.25	302.8
15.50	0.1757	3944.	5707.	7.24	304.7
16.00	0.1759	3936.	5702.	7.24	306.6
16.50	0.1760	3927.	5697.	7.23	308.5
17.00	0.1762	3919.	5692.	7.22	310.4
17.50	0.1763	3911.	5687.	7.22	312.3
18.00	0.1765	3903.	5682.	7.21	314.2
18.50	0.1766	3894.	5676.	7.20	316.0
19.00	0.1768	3886.	5671.	7.20	317.9
19.50	0.1770	3878.	5666.	7.19	319.8
20.00	0.1771	3870.	5661.	7.18	321.7
20.50	0.1773	3862.	5655.	7.18	323.5
21.00	0.1774	3855.	5650.	7.17	325.4
21.50	0.1776	3847.	5644.	7.16	327.3
22.00	0.1777	3839.	5639.	7.16	329.2
22.50	0.1779	3831.	5633.	7.15	331.0

RUN 2, TWALL=1100. TSAT=212. PRESS= 0. GFLUX= 18720. XEQ=0.1880 (RE)INLET= 4950.

DISTANCE	EQUILIBRIUM QUALITY	REYNOLDS NUMBER	HEAT FLUX	HEAT TRANSFER COEFFICIENT	VAPOR TEMPERATURE
		RESULTS USING ENTRANCE EFFECT CASE 2			
0.50	0.1885	4927.	16373.	18.44	216.8
1.00	0.1889	4892.	17357.	19.55	222.0
1.50	0.1893	4865.	14002.	15.77	226.1
2.00	0.1897	4841.	12384.	13.95	229.8
2.50	0.1900	4820.	10893.	12.27	233.0
3.00	0.1902	4801.	10022.	11.29	236.0
3.50	0.1905	4784.	9214.	10.38	238.7
4.00	0.1907	4768.	8716.	9.82	241.3
4.50	0.1910	4753.	8341.	9.39	243.8
5.00	0.1912	4738.	7968.	8.97	246.1
5.50	0.1914	4724.	7656.	8.62	248.4
6.00	0.1916	4711.	7406.	8.34	250.6
6.50	0.1918	4698.	7218.	8.13	252.7
7.00	0.1920	4686.	7092.	7.99	254.8
7.50	0.1922	4674.	7028.	7.91	256.9
8.00	0.1924	4661.	7025.	7.91	259.0
8.50	0.1926	4649.	7022.	7.91	261.0
9.00	0.1928	4637.	7019.	7.90	263.1
9.50	0.1929	4625.	7016.	7.90	265.2
10.00	0.1931	4613.	7013.	7.90	267.3
10.50	0.1933	4602.	7010.	7.89	269.4
		RESULTS USING ENTRANCE EFFECT CASE 3			
0.50	0.1885	4927.	16373.	18.44	216.8
1.00	0.1891	4878.	24421.	27.50	224.1
1.50	0.1895	4828.	26255.	29.57	231.8
2.00	0.1900	4785.	22516.	25.36	238.5
2.50	0.1904	4755.	16317.	18.37	243.3
3.00	0.1913	4732.	12599.	14.19	247.1
3.50	0.1916	4713.	10740.	12.09	250.2
4.00	0.1918	4696.	9500.	10.70	253.1

4.50	0.1921	4681.	8879.	10.00	255.7
5.00	0.1923	4666.	8259.	9.30	258.1
5.50	0.1925	4653.	7824.	8.81	260.4
6.00	0.1927	4640.	7451.	8.39	262.7
6.50	0.1929	4628.	7201.	8.11	264.8
7.00	0.1931	4616.	7014.	7.90	266.9
7.50	0.1933	4604.	7010.	7.89	268.9
8.00	0.1935	4592.	7007.	7.89	271.0
8.50	0.1937	4581.	7004.	7.89	273.1
9.00	0.1939	4569.	7000.	7.88	275.2
9.50	0.1941	4558.	6997.	7.88	277.2
10.00	0.1943	4547.	6993.	7.88	279.3
10.50	0.1945	4535.	6990.	7.87	281.4
11.00	0.1950	2280.	19784.	22.28	287.2
11.50	0.1955	2264.	19764.	22.26	293.1
12.00	0.1961	2249.	19744.	22.23	298.9
12.50	0.1963	4433.	6952.	7.83	301.0
13.00	0.1965	4422.	6947.	7.82	303.0
13.50	0.1967	4412.	6943.	7.82	305.1
14.00	0.1969	4402.	6938.	7.81	307.1
14.50	0.1970	4392.	6934.	7.81	309.2
15.00	0.1972	4382.	6929.	7.80	311.2
15.50	0.1974	4371.	6925.	7.80	313.3
16.00	0.1976	4362.	6920.	7.79	315.3
16.50	0.1978	4352.	6915.	7.79	317.4
17.00	0.1980	4342.	6910.	7.78	319.4
17.50	0.1982	4332.	6905.	7.78	321.5
18.00	0.1984	4322.	6900.	7.77	323.5
18.50	0.1986	4313.	6895.	7.76	325.6
19.00	0.1988	4303.	6890.	7.76	327.6
19.50	0.1989	4294.	6884.	7.75	329.6
20.00	0.1991	4284.	6879.	7.75	331.7
20.50	0.1993	4275.	6874.	7.74	333.7
21.00	0.1995	4266.	6869.	7.73	335.7
21.50	0.1997	4257.	6863.	7.73	337.8
22.00	0.1999	4247.	6857.	7.72	339.8
22.50	0.2001	4238.	6852.	7.72	341.8

RUN 3, TWALL=1200. TSAT=212. PRESS= 0. GFLUX= 18720. XEQ=0.1870 (RE)INLET= 4940.

DISTANCE	EQUILIBRIUM QUALITY	REYNOLDS NUMBER	HEAT FLUX	HEAT TRANSFER COEFFICIENT	VAPOR TEMPERATURE
		RESULTS USING ENTRANCE EFFECT CASE 2			
0.50	0.1875	4897.	18055.	18.27	217.4
1.00	0.1880	4859.	19157.	19.39	223.1
1.50	0.1884	4829.	15442.	15.63	227.7
2.00	0.1888	4803.	13653.	13.82	231.7
2.50	0.1892	4780.	12001.	12.15	235.3
3.00	0.1895	4759.	11037.	11.17	238.6
3.50	0.1897	4741.	10142.	10.27	241.6
4.00	0.1900	4723.	9591.	9.71	244.5
4.50	0.1903	4706.	9177.	9.29	247.2
5.00	0.1905	4691.	8763.	8.87	249.8
5.50	0.1907	4676.	8418.	8.52	252.3
6.00	0.1910	4661.	8142.	8.24	254.7
6.50	0.1912	4648.	7934.	8.03	257.1
7.00	0.1914	4634.	7796.	7.89	259.4
7.50	0.1916	4621.	7726.	7.82	261.7
8.00	0.1918	4608.	7724.	7.82	264.0
8.50	0.1920	4594.	7722.	7.82	266.3
9.00	0.1922	4582.	7720.	7.81	268.6
9.50	0.1924	4569.	7718.	7.81	270.9
10.00	0.1927	4556.	7716.	7.81	273.2
10.50	0.1929	4543.	7714.	7.81	275.5
		RESULTS USING ENTRANCE EFFECT CASE 3			
0.50	0.1875	4897.	18055.	18.27	217.4
1.00	0.1882	4844.	26998.	27.33	225.4
1.50	0.1890	4789.	29057.	29.41	234.1
2.00	0.1897	4741.	24923.	25.23	241.5
2.50	0.1902	4709.	18042.	18.26	246.8
3.00	0.1906	4684.	13915.	14.08	251.0
3.50	0.1909	4663.	11851.	11.99	254.5
4.00	0.1912	4644.	10475.	10.60	257.6

4.50	0.1915	4627.	9785.	9.90	260.5
5.00	0.1917	4612.	9097.	9.21	263.2
5.50	0.1920	4597.	8614.	8.72	265.8
6.00	0.1922	4584.	8201.	8.30	268.2
6.50	0.1924	4570.	7924.	8.02	270.6
7.00	0.1926	4558.	7716.	7.81	272.9
7.50	0.1928	4545.	7714.	7.81	275.2
8.00	0.1931	4532.	7712.	7.81	277.5
8.50	0.1933	4520.	7710.	7.80	279.8
9.00	0.1935	4508.	7707.	7.80	282.1
9.50	0.1937	4495.	7704.	7.80	284.4
10.00	0.1939	4483.	7702.	7.80	286.7
10.50	0.1941	4471.	7699.	7.79	289.0
11.00	0.1948	2245.	23183.	23.46	295.8
11.50	0.1954	2227.	23167.	23.45	302.7
12.00	0.1960	2210.	23149.	23.43	309.6
12.50	0.1962	4355.	7667.	7.76	311.9
13.00	0.1965	4344.	7663.	7.76	314.2
13.50	0.1967	4333.	7660.	7.75	316.5
14.00	0.1969	4322.	7656.	7.75	318.8
14.50	0.1971	4311.	7652.	7.74	321.0
15.00	0.1973	4300.	7647.	7.74	323.3
15.50	0.1975	4290.	7643.	7.74	325.6
16.00	0.1977	4279.	7639.	7.73	327.9
16.50	0.1979	4269.	7635.	7.73	330.1
17.00	0.1981	4258.	7630.	7.72	332.4
17.50	0.1983	4248.	7626.	7.72	334.7
18.00	0.1986	4238.	7621.	7.71	336.9
18.50	0.1988	4228.	7617.	7.71	339.2
19.00	0.1990	4217.	7612.	7.70	341.5
19.50	0.1992	4207.	7607.	7.70	343.7
20.00	0.1994	4197.	7602.	7.69	346.0
20.50	0.1996	4188.	7597.	7.69	348.2
21.00	0.1998	4178.	7592.	7.68	350.5
21.50	0.2000	4168.	7587.	7.68	352.8
22.00	0.2002	4158.	7582.	7.67	355.0
22.50	0.2004	4148.	7576.	7.67	357.3

RUN 4, TWALL=1300. TSAT=212. PRESS= 0. GFLUX= 18720. XEQ=0.1790 (RE)INLET= 4725.

DISTANCE	EQUILIBRIUM QUALITY	REYNOLDS NUMBER	HEAT FLUX	HEAT TRANSFER COEFFICIENT	VAPOR TEMPERATURE
		RESULTS USING ENTRANCE EFFECT CASE 2			
0.50	0.1795	4684.	19149.	17.60	218.0
1.00	0.1801	4643.	20333.	18.69	224.3
1.50	0.1805	4612.	16385.	15.06	229.4
2.00	0.1809	4584.	14485.	13.31	233.9
2.50	0.1813	4560.	12729.	11.70	237.8
3.00	0.1816	4539.	11705.	10.76	241.5
3.50	0.1819	4519.	10754.	9.88	244.8
4.00	0.1822	4501.	10168.	9.35	248.0
4.50	0.1825	4483.	9729.	8.94	251.0
5.00	0.1827	4467.	9289.	8.54	253.9
5.50	0.1830	4451.	8923.	8.20	256.7
6.00	0.1832	4436.	8630.	7.93	259.3
6.50	0.1834	4422.	8410.	7.73	262.0
7.00	0.1837	4408.	8263.	7.59	264.5
7.50	0.1839	4394.	8190.	7.53	267.1
8.00	0.1841	4380.	8189.	7.53	269.6
8.50	0.1843	4366.	8189.	7.53	272.2
9.00	0.1846	4353.	8188.	7.53	274.7
9.50	0.1848	4340.	8187.	7.53	277.2
10.00	0.1850	4326.	8186.	7.52	279.8
10.50	0.1852	4313.	8186.	7.52	282.3
		RESULTS USING ENTRANCE EFFECT CASE 3			
0.50	0.1795	4684.	19149.	17.60	218.0
1.00	0.1803	4627.	28687.	26.37	226.9
1.50	0.1812	4568.	30905.	28.40	236.5
2.00	0.1819	4519.	26517.	24.37	244.7
2.50	0.1824	4485.	19188.	17.64	250.7
3.00	0.1828	4459.	14790.	13.59	255.3
3.50	0.1832	4437.	12590.	11.57	259.2
4.00	0.1835	4418.	11123.	10.22	262.7

4.50	0.1838	4400.	10389.	9.55	265.9
5.00	0.1840	4384.	9656.	8.87	268.9
5.50	0.1843	4369.	9142.	8.40	271.7
6.00	0.1845	4354.	8701.	8.00	274.4
6.50	0.1848	4341.	8407.	7.73	277.0
7.00	0.1850	4327.	8186.	7.52	279.6
7.50	0.1852	4314.	8186.	7.52	282.1
8.00	0.1854	4301.	8185.	7.52	284.7
8.50	0.1857	4288.	8184.	7.52	287.2
9.00	0.1859	4276.	8182.	7.52	289.8
9.50	0.1861	4263.	8181.	7.52	292.3
10.00	0.1863	4250.	8179.	7.52	294.9
10.50	0.1866	4238.	8178.	7.52	297.4
11.00	0.1873	2125.	26591.	24.44	305.7
11.50	0.1880	2105.	26580.	24.43	313.9
12.00	0.1888	2086.	26566.	24.42	322.2
12.50	0.1890	4110.	8153.	7.49	324.7
13.00	0.1892	4099.	8150.	7.49	327.3
13.50	0.1894	4088.	8147.	7.49	329.8
14.00	0.1897	4076.	8144.	7.49	332.3
14.50	0.1899	4065.	8141.	7.48	334.8
15.00	0.1901	4055.	8138.	7.48	337.4
15.50	0.1903	4044.	8135.	7.48	339.9
16.00	0.1905	4033.	8131.	7.47	342.4
16.50	0.1908	4022.	8127.	7.47	345.0
17.00	0.1910	4012.	8124.	7.47	347.5
17.50	0.1912	4001.	8120.	7.46	350.0
18.00	0.1914	3991.	8116.	7.46	352.5
18.50	0.1917	3980.	8112.	7.46	355.1
19.00	0.1919	3970.	8108.	7.45	357.6
19.50	0.1921	3960.	8103.	7.45	360.1
20.00	0.1923	3950.	8099.	7.44	362.6
20.50	0.1926	3940.	8095.	7.44	365.1
21.00	0.1928	3930.	8090.	7.44	367.6
21.50	0.1930	3920.	8086.	7.43	370.2
22.00	0.1932	3910.	8081.	7.43	372.7
22.50	0.1934	3901.	8076.	7.42	375.2

APPENDIX E: WATER AND VAPOR PROPERTIES

TABLE 2: SYSTEM PROPERTIES

WATER

$$\rho_L = 60 \quad lbm/ft^3$$

$$(Cp)_L = 1 \quad Btu/lbm°F$$

STEAM

$$\rho_v = .04559 - .00003958 \times T_{vap} \quad lbm/ft^3$$

$$K_v = .00747 + .0000551 \times T_{vap} \quad Btu/Hr\text{-}ft\ °F$$

$$\mu_v = .01747 + .0000551 \times T_{vap} \quad lbm/hr\text{-}ft$$

$$(Cp)_v = .48 \quad Btu/lbm°F$$

$$Pr_v = \frac{(Cp)_v \times \mu_v}{K_v}$$